



UNIVERSITÀ
DEGLI STUDI
DI PADOVA

UNIVERSITA' DEGLI STUDI DI PADOVA

Dipartimento di Ingegneria Industriale DII

Corso di Laurea Magistrale in Ingegneria Energetica

Tesi di Laurea Magistrale

Simulation of a district heating case study in
Aalborg

Relatore: Angelo Zarrella

Correlatore: Marco Cozzini (Eurac Research)

Andrea Benedetti 1234075

Anno Accademico 2021/2022

Abstract

District heating and cooling (DHC) networks play a fundamental role in the transition towards a sustainable supply of heating and cooling, due to their ability to integrate any available source of thermal energy and to distribute it to the buildings. The possibility of recovering waste and renewable heat in urban areas has made district heating networks one of the key infrastructures for decarbonising the heating sector in Europe.

An example of such systems is presented in this paper: part of a network located in Aalborg (Denmark), that mainly recovers waste heat from a cement factory has been analysed with the simulation tool *NeMo*, a steady state hydraulic and transient thermal model, developed by the University of Padua, which predicts the behaviour of district heating networks. Before tackling the simulation of this real case, the accuracy of the tool has been examined by means of an ideal simplified case study consisting of three pre-insulated single pipes, comparing the results with a MATLAB-based theoretical solution, and with another simulation tool developed by Eurac Research, highlighting the differences among them.

The analysis of the Aalborg network has then been carried out based on load estimated through the EURECA tool. Thermal losses and return temperature have been assessed. Moreover, a clustering work has been completed for the considered network, composed of 158 nodes and 157 branches, reducing the number of elements by about 15%. This cut contributes to reduce the computational effort of such models, in order to decrease the simulation time, as in this case, from 27 to 20 minutes.

The clustering method used in this work is based on the Danish Method, taken from the literature, which allows to conserve the same features of the original network such as thermal power, mass flow rate, water volume and heat losses, without conserving the length of the pipes in the equivalent one, by using two steps, implemented in MATLAB as functions.

This work will contribute to part of the project LIFE4HeatRecovery, contract nr. LIFE17_CCM/IT/000085, a European project funded by the LIFE Programme and focused on low-temperature waste heat recovery in district heating and cooling networks.

Abstract

Le reti di teleriscaldamento stanno svolgendo un ruolo fondamentale nella transizione verso la sostenibilità di sistemi di riscaldamento e raffrescamento, grazie all'opportunità di integrazione con qualsiasi risorsa disponibile di energia termica e di renderla disponibile servendo gli edifici. La possibilità di recuperare calore di scarto ed energia da rinnovabile in aree urbane ha reso il teleriscaldamento una delle infrastrutture chiave per la decarbonizzazione relativa al settore di riscaldamento domestico in Europa.

Un esempio di questi sistemi è presentato in questo lavoro: una parte di una rete di teleriscaldamento localizzata ad Aalborg (Danimarca), che recupera calore di scarto principalmente da un cementificio è stata analizzata tramite il modello di simulazione NeMo, ovvero un modello idraulico stazionario e termico transitorio, sviluppato dall'Università di Padova, che esegue una previsione del comportamento di reti di teleriscaldamento. Prima di affrontare la simulazione del caso reale, l'accuratezza di questo modello è stata esaminata mediante un caso studio ideale semplificato, il quale consisteva di tre singoli tubi pre-isolati connessi tra loro, paragonando i risultati con una soluzione teorica sviluppata in MATLAB e con un altro modello di simulazione sviluppato da Eurac Research, evidenziandone le differenze tra i due.

L'analisi della rete di Aalborg è stata effettuata grazie ad una stima fittizia dei carichi termici attraverso il software EURECA. Le perdite termiche e le temperature di ritorno sono state esaminate successivamente. Inoltre, è stato effettuato un lavoro di clusterizzazione per la rete intera, composta da 158 nodi e 157 rami, riducendo il numero di elementi di circa il 15%. Questa rimozione ha contribuito alla riduzione dello sforzo computazionale a cui si prestano questi modelli, in modo tale da diminuire il tempo impiegato dalla simulazione, in questo caso, da 26.69 minuti a 20 minuti.

Il metodo di clusterizzazione applicato in questa tesi è basato sul metodo Danese, tratto dalla letteratura, che permette di conservare le caratteristiche principali della rete originale nella rete equivalente, come potenza termica, portata, volume totale di acqua e perdite termiche, ma senza conservare la lunghezza originale dei tubi, attraverso l'applicazione di due step, implementati come funzioni in MATLAB.

Questo lavoro contribuirà ad una parte del progetto LIFE4HeatRecovery, numero di contratto LIFE17_CCM/IT/000085 il quale è un progetto Europeo fondato da LIFE Programme, focalizzato sul recupero di calore a bassa temperatura in reti di teleriscaldamento e teleraffrescamento.

Contents

1. Introduction.....	1
1.1 Overview of the DHC generations.....	2
1.2 Overview of the DHC physical model.....	6
1.3 Clustering.....	7
2. Models	9
2.1 <i>NeMo</i> model.....	9
2.1.1 The hydraulic balance.....	10
2.1.2 The thermal balance	12
2.1.3 Input, Output	14
2.2 Detailed Model.....	16
Input, Output.....	18
3. Case study	21
3.1 Ideal simplified case study.....	21
3.2 Real case study - Aalborg DHN.....	22
4. Methodology.....	25
4.1 Ideal simplified case study.....	25
4.1.1 <i>NeMo</i>	29
4.1.2 Detailed Model.....	33
4.2 Real case study: Aalborg DHN.....	36
4.2.1 <i>NeMo</i> inputs	36
<i>EUReCA</i> : Energy Urban Capacitance Approach.....	36
Loads, Mass Flow Rate, Supply and Ground Temperature	45
Parameters	53
5. Clustering.....	55
5.1 Collapsing a network tree into one branch – step 1.....	55
5.2 Removing internal nodes – step 2.....	60
6. Results	66
6.1 Original case study.....	66
6.2 Clustered case study	70

7. Conclusions	77
References	79
Appendix	82
Ringraziamenti	92

List of Figures

Chapter 1

Figure 1.1: Illustration of the concept of 4 th Generation District Heating in comparison to the previous three generations.....	4
---	---

Chapter 2

Figure 2.1: Structure of NeMo.	10
Figure 2.2: Control volume of the i-th node.....	13
Figure 2.3: NeMo interface MATLAB App: a) Input, b) Parameters, c) Output.	16

Chapter 3

Figure 3.1: Aalborg DHN.	23
-------------------------------	----

Chapter 4

Figure 4.1: : Theoretical solution with a) 35 mm thickness, b) 5 mm thickness....	28
Figure 4.2: NeMo outlet temperature profiles for $Co=0.8$ fix.	32
Figure 4.3: NeMo outlet temperature profiles for $\Delta\tau=15$ s fix.....	33
Figure 4.4: Definition of the Detailed Model new parameter ΔL	34
Figure 4.5: Detailed Model outlet temperature profiles for different value of max <i>nparticles</i>	35
Figure 4.6: QGIS buildings, nodes, pipes layer.	38
Figure 4.7: Thermal power profiles for diverse types of buildings.	43
Figure 4.8: Maximum thermal power per hours for all the buildings.	43
Figure 4.9: Annual energy consumption for every ID buildings.	44
Figure 4.10: Thermal peak power for every ID buildings.....	45
Figure 4.11: Example of association between buildings and node 42.....	46
Figure 4.12: Outdoor temperature profile.....	49
Figure 4.13: Climatic curve for the supply temperature of the supply station.	49
Figure 4.14: Ground temperature profile compared to the surface, average, and outdoor one.	52

Chapter 5

Figure 5.1: Collapse of the branch 1 in the branch 2 – step 1.....	55
Figure 5.2: Removing internal nodes – step 2.	60
Figure 5.3: Starting configuration of the North-West part of DHN.	63
Figure 5.4: Following step 1 (collapsing node) to align the nodes and pipes for step 2 (removing internal nodes).	64

Chapter 6

Figure 6.1: Different profiles of supply and return temperature among supply station and node 48.....	66
Figure 6.2: Representation of thermal inertia of the fluid in the changing of supply temperature by supply station.....	67
Figure 6.3: Node 48 temperature drop related to the distance from supply station.....	68
Figure 6.4: Weekly heat losses of the whole network.	69
Figure 6.5: Linear trend of the network heat losses related to the supply temperature of the supply station.	69
Figure 6.7: Supply and return profiles temperature of node 39 (ex 48) and supply station for the equivalent network.	72
Figure 6.8: Comparison between temperature drop of old node 48 and new node 39 (ex 48) related to the distance.....	73
Figure 6.9: Comparison of thermal inertia term between the original and equivalent networks.	74
Figure 6.10: Comparison between monthly heat losses between original and equivalent networks.	74
Figure 6.11: Computational time taken by NeMo for a) Original network, b) Equivalent network.....	75

List of Tables

Chapter 3

Table 3.1: Characteristics of the ideal simplified case study.....	21
--	----

Chapter 4

Table 4.1: Amount of heat losses [kW] for different inlet temperature.....	29
Table 4.2: Definition of Loads.xlsx input file.....	30
Table 4.3: Definition of Subs.xlsx input file.	30
Table 4.4: a) Incidence Matrix, b) Characteristics of the pipes.	30
Table 4.5: Definition of Ground.xlsx input file.....	31
Table 4.6: Definition of the Parameters.xlsx input file.....	31
Table 4.7: Different week schedules for type of buildings.	41
Table 4.8: Different weekend schedules for type of buildings.	42
Table 4.9: Association between buildings and nodes of the DHN West part. ...	47
Table 4.10: Association between buildings and nodes of the DHN East part. ...	47
Table 4.11: Statistic results for the constant ΔT assumption.	50
Table 4.12: Parameters of the simulation.....	53

Chapter 6

Table 6.1: ID of nodes and pipes removed from the original network.....	71
Table 6.2: Conserved properties between original and equivalent network.....	71

Nomenclature

DH: District Heating

DHN: District Heating Network

DHC: District Heating and Cooling

LTDH: Low Temperature District Heating

CHP: Combined Heat and Power

RHC: Renewable Heating and Cooling

DHW: Domestic Hot Water

WSHP: Water-Source Heat Pump

Avg: average

SC: Space Cooling

nn: Number of nodes

nb: Number of branches

PU: Polyurethane

PE: Polyethylene

AHU: Air Handling Unit

T_s or T_{sup} : Supply Temperature

T_r or T_{ret} : Return Temperature

T_{out} : T_{outlet}

T_G or T_g : Ground Temperature

Chapter 1

Introduction

‘District heating (DH) comprises a network of pipes connecting the buildings in a neighbourhood, town centre or whole city, so that they can be served from centralised plants or several distributed heat producing units. This approach allows any available source of heat to be used’

In the transition to sustainable cities, district heating networks (DHNs) plays a crucial role, as their inclusion allows for the wide use of combined heat and power (CHP) together, with the utilisation of heat from waste-to-energy and various industrial surplus heat sources as well as the inclusion of geothermal and solar thermal heat, to provide space heating and domestic hot water to buildings.^{1,2}

European energy policy relies on the construction and expansion of efficient DH systems, since almost half of the final energy consumed in Europe is related to heating services.³ Moreover, improving the design and operational aspects of DHNs is important to increase the efficiency of the systems from both an economic and an ecological perspective.

As far as design aspects are concerned, Lund et al.⁴ have developed the concept of low temperature district heating (LTDH), or 4th generation district heating (4GDH). This concept aims to abate heat losses in the distribution system by reducing the supply temperature and integrating low-grade unconventional heat sources (renewable energy and low temperature waste heat) in the network. The step towards 4th generation DH systems has been driven by the reducing trend of heat demand that is expected to continue during next decades due to the progressive refurbishment of existing buildings and to the high energy performance of new buildings. In fact, the RHC Technology Platform estimates different trends in thermal energy consumptions in Europe by 2050, with a reduction in the heating demand between 20% and 30% and a rise of about three times of the cooling demand compared to 2006 values.⁵ Furthermore, this tendency is confirmed by the 600% increase of the cooled floor area assessed in the EU between 1990 and 2010.⁶ Moreover, the number of space cooling (SC) units installed in the same period, dominated by room air conditioners, expanded by 24 times with a growth rate of 3% per year.

Traditional DH systems consist of centralised power stations that feed hot water or steam into pipes to distribute heat in urban areas. High-temperature DH systems still suffer from significant heat losses and high installation costs. Especially in summer, when generally many DH systems operate only to meet the DHW demand, the network thermal losses can reach a value of about 30% of the supplied energy because of the high retention time of water in the network. Prando et al. (2015) argue that the economic profitability of traditional high-temperature DH infrastructures can be compromised by these issues together with the reduction in heating demand due to the renovation rate of the existing building stock.⁷ For these reasons, current research focuses on the 4th and 5th Generation DHC networks, which can reach high efficiencies by operating at low temperatures.

The competitiveness of district heating derives from a combination of the conditions for heat supply and heat distribution. One important condition for heat distribution is that the heat demands must be concentrated in order to minimise distribution costs and heat losses.⁸ Low heat densities in sparse areas lead to relatively higher distribution costs and losses.^{9,10} Of fundamental importance when making strategic longer-term choices is the fact that the major Central European cities are dense enough to handle a major reduction in the customer heat demands without losing the overall competitiveness of district heating.

1.1 Overview of the DHC generations

In general, DHC systems are a viable solution to provide heating and cooling in urban environments.

In this section an overview about the first four generations of district heating and cooling systems is presented.¹¹

First generation – 1GDH

The first generation of DH systems used steam as heat carrier. These systems were first introduced in USA in the 1880s. All district heating systems established until 1930 used this technology, all around the world. Typical components were steam pipes in concrete ducts, steam traps, and compensators. Nowadays such systems using steam can be considered an outdated technology: high steam temperatures could generate consistent heat losses and severe accidents, as explosions, while condensate return pipes can be often corroded, ensuring a lower overall efficiency. These systems showed up with the aim of presenting themselves as a valid

alternative to the individual boilers in apartment buildings, due to the risk of explosion reduction and greater comfort. The main part of heat was delivered by steam condensation in radiators at the consumers.

Second generation – 2GDH

The second generation of DH systems used pressurised hot water as the heat carrier, with supply temperatures mostly over 100°C. Mainly used in Soviet Union, DH systems were first introduced in the 1930s and they have remained the most used until the 1970s. Typical components were water pipes in concrete ducts, large tube-and-shell heat-exchangers and material-intensive, large and heavy valves. On the one hand, this technology allowed to achieve fuel savings and better comfort by utilising CHP, which was in some cases adopted in urban areas. On the other hand, the quality was poor and lacked any heat demand control.

Third generation – 3GDH

The third generation of DHC systems, often associated with ‘Scandinavian district heating technology’, was introduced in the 1970s, but only in the 1980s and beyond it spreads and became a viable alternative. Pressurized water is still the heat carrier, but the supply temperatures are often below 100°C. Typical components are prefabricated, pre-insulated pipes directly buried into the ground, compact substations using plate stainless steel heat exchangers, and material lean components. As specified by Lund et al., 2014, "the primary motivation of this system is security of supply in relation to the two oil crises leading to a focus on energy efficiency related to CHP and replacing oil with various local and/or cheaper fuels such as coal, biomass and waste. Moreover, solar and geothermal heat has been used a supplement in a few places".

Fourth generation – 4GDH

Fourth generation of DH technology comprises lower distribution temperatures, assembly-oriented components and more flexible pipe materials. In other words, it follows the already outlined trend towards lower distribution temperatures, material lean components and prefabrication, leading to reduced manpower requirements at construction sites. According to Lund et al., 2014, “this generation uses high shares of all kinds of renewable energy into the central generation plants by providing high flexibility to the electricity system”.

In the following list, some key features of fourth generation DH systems are shown, according to Lund et al., 2014:

- The system should supply low-temperature (50-60°C) district heating for space heating and domestic hot water to all type of buildings.
- Low grid losses during the distribution of heat.
- Ability to recycle heat from low-temperature sources and integrate renewable heat sources in the system such as geothermal and solar.
- The system should be part of a smart energy system, i.e., a thermal grid, furthermore, this should include being an integrated part of a district cooling system.
- It must ensure suitable planning cost and motivation structures in relation to the operation as well as to strategic investments related to the transformation into future sustainable energy systems.

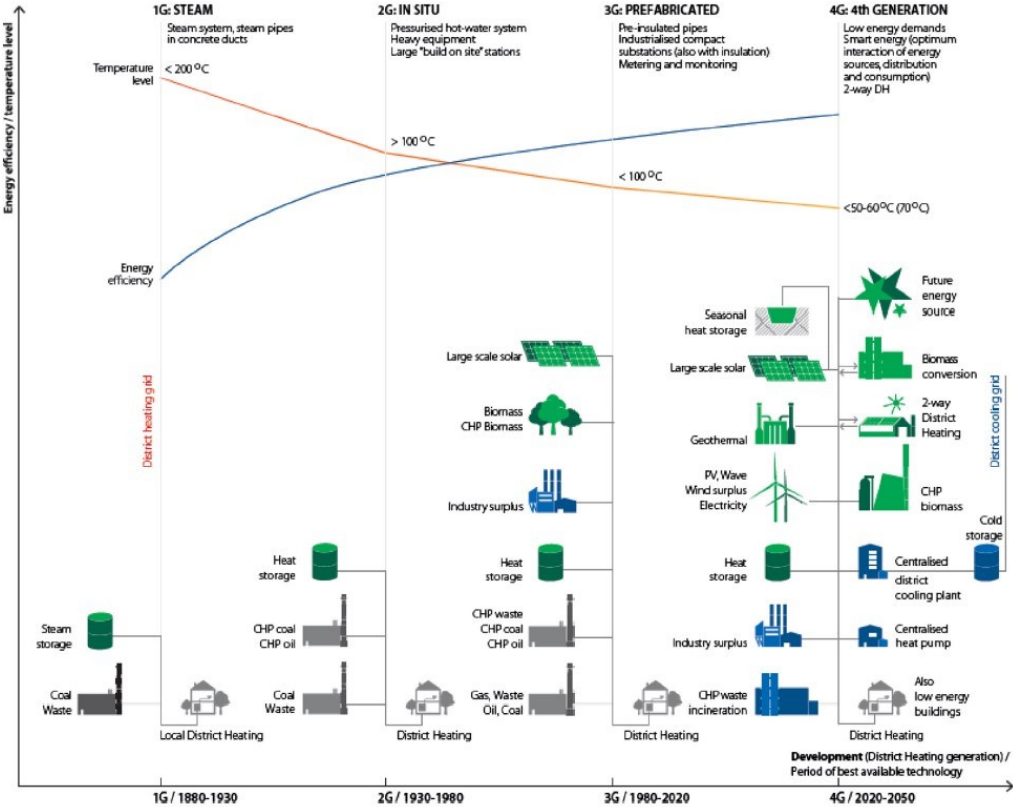


Figure 1.1: Illustration of the concept of 4th Generation District Heating in comparison to the previous three generations.

The real case study of Aalborg analysed in this work is considered as third generation DHN.

Fifth generation – 5GDHC

Neutral-Temperature or *5th* Generation District Heating and Cooling (5GDHC) network is an innovative concept of DHC systems: it combines the properties of local renewable energy systems with the principles of future DH.¹²

While conventional DH systems have a linear design, where heat is generated at a source and transported to the consumers using hot water, with a return flow of water, which has no value from an energy perspective, a 5GDHC system is non-linear, bidirectional, and decentralized. It does not have return flows as such, but warm and cold pipes.

With 4GDH, same pipes cannot simultaneously provide heating and cooling services to different buildings, so that, the born of 5GDHC technology overcomes this problem. Despite 5GDHC networks are at the early stage of development, several systems are in operation in Europe mainly started as pilot projects. Many of these systems operate differently from traditional DHC technology, as they supply water to decentralised Water-Source Heat Pumps (WSHP) at a temperature in the range between 0 °C and 30 °C. This has several advantages compared to traditional DH systems, as presented in the previous section. Moreover, 5GDHC permits a free-floating temperature of the network and the exploitation of quasi-infinite indigenous heat sources. Distribution temperature close to the ground one (“neutral” from thermal losses point of view), the capability to work in heating or cooling mode independently of network temperature, bi-directional and decentralised energy flows are some of the keys added values of 5GDHC relating to 4GDH.

Progetto LIFE4HeatRecovery

LIFE4HeatRecovery¹³ is a European project that involve different country such as Italy, Germany, Netherlands, and Denmark. It demonstrates the recovery of urban waste heat available at low temperature (<40°C), in highly efficient district heating and cooling networks operated at conventional or low temperature. This is done by means of heat pumps used either at heat recovery or heat utilization sides, with a focus on prefabricates solutions.

LIFE4HeatRecovery networks will pursue the following objective:

- To demonstrate opportunity and effectiveness of waste heat recovery from multiple urban sources,
- To demonstrate management strategies for DH network,

- To demonstrate trading schemes allowing to manage thermal energy fed/purchased by/from different customers,
- To develop financial schemes enabling large public and private investments to be mobilized.

Three demo-cases are included:

- Ospitaletto, Italy: LGDH, industrial waste heat sources,
- Aalborg, Denmark: Conventional network, industrial and Data Centre waste heat sources,
- Herleen, Netherlands: experimental demo-case.

This work is focused on the demo-case of Aalborg.

1.2 Overview of the DHC physical model

The modelling of DH systems represent a key phase to understand the thermal and hydraulic behaviour in different operating conditions.

The element method and the node-method are both models that can be used as means of simulating transient thermal behaviour in district heating systems.¹⁴

The element method solves the transient heat balance equation by means of different possible finite difference schemes. Low-order schemes suffer from artificial numerical diffusion, causing abnormal smoothing of sharp temperature profiles¹⁵, while higher-order schemes may result in overshooting.¹⁶

In the element method, the temperature at each time-step is determined only from the time-step before, while the node method, uses temperature values at different time-steps to determine the current temperature situation.

Palsson et al. implemented and assessed two models based on the different two methods. In the comparison, the node method was found to be superior to the element method at low Courant numbers, unless schemes of higher order are employed, which corresponds to the situation with long district heating pipes and sharp temperature gradients that require small time steps.

Furthermore, the computational effort is also lowered for the node-method, but the application of the node method is however limited to tree-shaped networks.¹⁷

A new numerical approach to model the heat transmission over long pipes has been presented by Denarie et al.¹⁸ The model is based on the method of characteristics, and it splits the water thermal capacitance between the turbulent

core and the boundary layer. Further modelling studies have been conducted on the temperature dynamics in variable flow DHN.

Duquette et al.¹⁹ have built a pipe model using a steady state heat transfer model combined with a variable transport delay. Stevanovic et al.²⁰ have presented a model of the Zemun district heating network in Serbia able to analyse thermal transients and fluid propagation time delays from source to consumers in the entire system. In order to realize fast and accurate calculations, Wang et al.²¹ have investigated the optimal time and spatial steps to use in DHN models.

The work presented in this thesis rely on the accuracy of a steady-state hydraulic and transient thermal model called *NeMo*, developed by the University of Padua, to reproduce the hydraulic and thermal behaviour of district heating networks.

In the ideal case study, presented in the section 3.1, the accuracy of the model has been investigated reproducing the heat waves along a single pipe. The results proved that the heat propagation through the network can be accurately reproduced, provided that the network is correctly discretized. The model is similar to that developed at Polytechnic of Turin, which was used for studying both thermal and hydraulic behaviour of complex thermal networks.

Compared to other models, *NeMo* allows to discretize the considered DHN in time and space ex ante, without modifying its geometrical and topological features.

1.3 Clustering

This physical models, like *NeMo* and the others mentioned so far, often represent the whole structure of the DH system involved, and it is, therefore, easy to change or add new components to an existing model. Since these models require a full description of the DH system, they tend to be, computationally, very intensive. Thus, in order to reduce this intensity, it might be desirable to simplify the physical description without losing the relation of the model to the real pipe network in consideration, generating an equivalent network with the same features of the original one.²²

The process useful to obtain an equivalent network explained above is called *clustering*.

The clustering method, exploited in the chapter 5 for the Aalborg network, is called Danish Method²³, taken from the literature, and implemented, as functions of each steps, in MATLAB.

Chapter 2

Models

In this chapter are presented the generality (structure, hydraulic and thermal balances, input, and output) of the two simulation tools NeMo and Detailed Model used to analyse the ideal case study reported in chapter 3. The real case study has been examined only with NeMo model.

2.1 *NeMo* model

NeMo is a MATLAB steady-state hydraulic and transient thermal model, developed by the University of Padua, to reproduce the hydraulic and thermal behaviour of district heating networks, in order to give in output the branches mass flow rates, the supply and return pressure and the supply and return temperature of the nodes.

NeMo describes the topology of the network using graph theory. The network is represented by a set of nodes and oriented branches and an adjacency matrix determines their mutual connections.

A slug flow is assumed, which implies that the velocity of the heat carrier fluid is uniform in the radial direction (one dimensional model). In problems of forced convection, the velocity of the heat carrier fluid does not depend on the temperature distribution. Therefore, the hydraulic and thermal problems can be uncoupled. This allows performing the calculation of the mass flow rates and the pressures across the network in a first step; then, given the mass flow rates, the energy balance is solved to find out the temperature distribution.

The overall structure of the model is illustrated in Fig. 2.1.

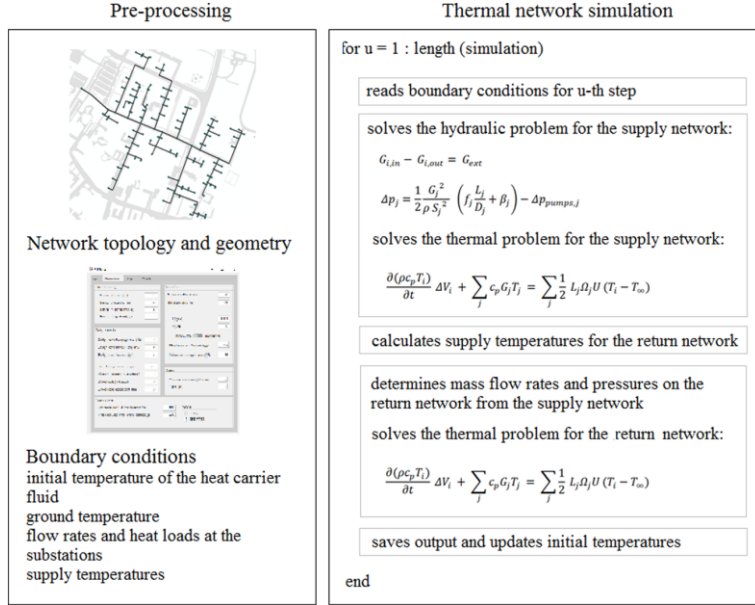


Figure 2.1: Structure of NeMo.

2.1.1 The hydraulic balance

Modern DH systems use pressured water as the heat carrier, so two equations can be exploited to describe the flow and pressure distribution: the continuity equation and the momentum equation. Eq. (2.1) applies the law of conservation of mass to the i -th node of the network:

$$G_{i,in} - G_{i,out} = G_{i,ext} \quad (2.1)$$

where $G_{i,ext}$ is the $nn \times 1$ vector of mass flow rates exiting/entering the system from/in the nodes. The Navier-Stokes equations (2) are applied to the j -th branch of the network, including both distributed and concentrated pressure losses respectively due to viscosity and geometrical irregularities:

$$\Delta p_j = \frac{1}{2} \rho \left(f_j \frac{L_j}{D_j} + \sigma_j \right) v_j^2 - \Delta p_{pump,j} \quad (2.2)$$

Velocity are connected to mass flow rate through Eq.3:

$$G_j = \rho S_j v_j \quad (2.3)$$

By substituting (2.3) in (2.2) the following holds true:

$$\Delta p_j = r_j G_j^2 - \Delta p_{pump,j} \quad (2.4)$$

Where all the constant terms that refer to the j -th pipe are grouped into the constant r :

$$r_j = \frac{1}{2\rho S_j^2} \left(f_j \frac{L_j}{D_j} + \sigma_j \right) \quad (2.5)$$

Thus, all mass flow rates and pressures can be found by solving two systems of equations that can be written in matrix form as:

$$\mathbf{A}\dot{\mathbf{G}} + \dot{\mathbf{G}}_{ext} = 0 \quad (2.6)$$

$$\mathbf{A}^T \mathbf{P} = r \dot{\mathbf{G}}^2 - h \quad (2.7)$$

Where \mathbf{G} and \mathbf{P} are the $nb*1$ vector of mass flow rates and the $nn*1$ vector of pressures, respectively. The heads provided by the pumps $\Delta p_{pump,j}$ are stored in the $nb*1$ vector h . Thus, the overall system has $nn + nb$ equations and the same number of unknown variables. These systems are coupled because G appears in both equations. Moreover, the overall system is nonlinear because the pressure drops depend on the square of the flow rates.

In order to solve the whole system represented by 2.6 and 2.7, the model uses the semi-implicit method for pressure linked equations, also known as Simple Method [41]. This method involves first calculating an intermediate velocity field based on an estimated pressure field, and then applying appropriate corrections to determinate the pressure field and satisfy the continuity equation. The momentum equation is linearized by expressing the first term as product of a hydraulic resistance R (expressed in (2.5) and of the mass flow rate G . Therefore Eq. 2.4 can be rewritten as:

$$\Delta p_j = R_j G_j - \Delta p_{pump,j} \quad (2.8)$$

In matrix notation:

$$\mathbf{A}^T \mathbf{P} = R(\dot{\mathbf{G}})\dot{\mathbf{G}} - h \quad (2.9)$$

A guess-value vector for mass flow rates is used to calculate the nb^*nb diagonal matrix of hydraulic conductance, Y , where $Y_{j,j} = 1/R_j$. Then, a guess-value vector for pressures \mathbf{P}^* is assumed and used to calculate a new vector of mass flow rates \mathbf{G}^* in Eq.10. The latter equation is obtained by left-multiplying both members of (2.9) by Y :

$$\mathbf{G}^* = Y\mathbf{A}^T\mathbf{P}^* + Yh \quad (2.10)$$

With this vector \mathbf{G}^* , the new conductance matrix Y^* can be estimated. Then, if $Y = Y^*$ and using (2.6), both pressures and flows can be corrected simultaneously:

$$\mathbf{A}Y^*\mathbf{A}^T\Delta P^{corr} = -\mathbf{A}\mathbf{G}^* - G_{ext} \quad (2.11)$$

$$\Delta G^{corr} = Y^*\mathbf{A}^T\Delta P^{corr} \quad (2.12)$$

The pressure correction can be obtained by solving the linear system represented by (2.11). Then, the resulting vector can be used to calculate the mass flow rate correction, as shown in (2.12). Finally, under-relaxation factors can be used to calculate the new vectors of G and P that can be used as inputs for the next iteration. The iteration loop ends when the norm of the residuals of both G and P are lower than a tolerance –in this case set to 0.01 kg/s and 50 Pa, respectively. Since the momentum equation provides pressure differences, the pressure in one node must be fixed as boundary condition. After the convergence, the guess vectors for pressures and mass flow rates are updated using those of the previous time-step in order to reduce the computation time.

2.1.2 The thermal balance

The heat propagation in the network is described by the energy balance performed on the volume of the heat carrier fluid around the nodes of the network. The control volume of the i -th node corresponds to half of the heat carrier fluid volume of all the branches connected to it as shown in Fig. 2.2:

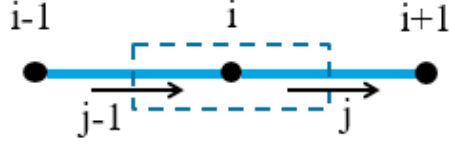


Figure 2.2: Control volume of the i -th node.

The model neglects the heat conduction through the wall pipe along the axial direction; the heat transfer in the radial direction considers the convection between the heat carrier fluid and the inner pipe surface, the thermal resistance of the pipe and its thermal insulation, as well as the thermal resistance of the surrounding ground. The thermal capacitance of the surrounding ground is not considered. Applying the energy balance to the node shown in Fig. 2.2 leads to (2.13):

$$\rho V_i c_p \frac{\partial T_i}{\partial t} = G_{j-1} c_p T_{j-1} - G_j c_p T_j - \frac{1}{2} (L_j \Omega_j U_j + L_{j-1} \Omega_{j-1} U_{j-1}) (T_i - T_g) \quad (2.13)$$

Where G is the mass flow rate, V is the volume of the heat carrier fluid enclosed in the control volume, Ω is the perimeter of the pipe section, U is the radial heat transmission coefficient from fluid to the ground and the T_g is the undisturbed ground temperature. The temperature of the branches is then associated to the temperature of the corresponding upwind nodes, according to the well-known upwind scheme. Therefore, (2.13) becomes:

$$\rho V_i c_p \frac{T_i^t - T_i^{t-\Delta t}}{\Delta t} = G_{j-1} c_p T_{i-1}^t - G_j c_p T_i^t - \frac{1}{2} (L_j \Omega_j U_j + L_{j-1} \Omega_{j-1} U_{j-1}) (T_i^t - T_g) \quad (2.14)$$

(2.14) can be represented in matrix form as:

$$\mathbf{M}\dot{\mathbf{T}} = \mathbf{s} - \mathbf{K}\mathbf{T} \quad (2.15)$$

where M and K are the so-called mass matrix and stiffness matrix, respectively. The temperature at the inlet node is fixed (Dirichlet condition). In a previous version of the software, the first-order ordinary differential equation (ODE) was formulated as by (2.15) and solved by MATLAB's ODE solver ode15s which implements the Numerical Differentiation Formulas (NDF). This formulation was discarded because the ODE solvers do not allow to set the calculation time-step. Therefore, (2.15) was linearised as follows:

$$\frac{\mathbf{M}}{\Delta t}(T - T_0) = s - \mathbf{K}T \quad (2.16)$$

Where T_0 represents the temperature vector of length nn with the temperature values of the preceding time-step (initial network temperature at the beginning of the simulation). (2.16) can then be rewritten in the classical form of a linear system ($Ax = b$) as follows:

$$\left(\mathbf{K} + \frac{\mathbf{M}}{\Delta t}\right)T = \left(s + \frac{\mathbf{M}}{\Delta t}T_0\right) \quad (2.17)$$

The linear system of Eq. (2.17) can then be solved with Gauss-elimination methods. The mass matrix is zero at the inlet nodes in order to set the temperature at the system boundaries (Dirichlet condition); the missing mass is attributed to the adjacent nodes.

In the current version of the model *NeMo*, the user is free to choose the resolution method for the transient heat propagation problem between the ODE solver and the linear system solver. The latter requires the user to set the internal calculation time-step Δt .

2.1.3 Input, Output

The MATLAB *NeMo* App, Fig. 2.3, requires several input to run the simulation of the DHN.

All the input are set as Excel files, except for the *Parameters* file, which can be prepared using the related interface of the MATLAB App.

The input files are presented as follow:

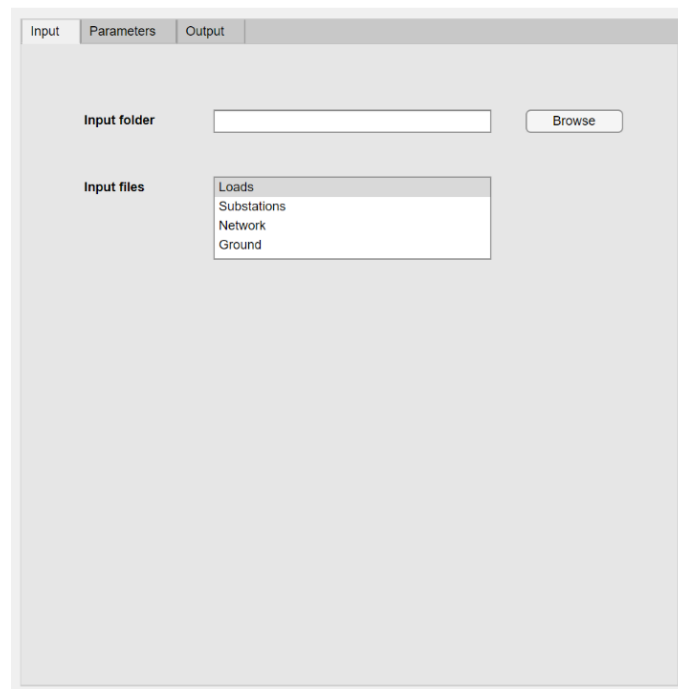
- The first one is called HeatLoads, in which are reported three spreadsheets regarding the thermal power [kW] and the mass flow rate [kg/s] of the substations linked to the input time step (usually, 1 hour is chosen), and lastly the supply station temperature, always related to the same input time-step.
- The second file regards the clarifying of ID supplier nodes and the ID consumer nodes.
- The third file deals with the topology of the network and contains the spreadsheets of the incidence matrix and the characteristics of the ducts.

- The fourth file is about the undisturbed ground temperature associated to the same input time-step considers previously.
- The latter file is a simulation parameters file, which clarify the chosen input time-step, the total simulation time (sum of the input time step), the initial supply temperature, the tolerance of the hydraulic and thermal balance to reach the convergence and other similar parameters.

With those input Excel files, the output folder obtained are the following:

- The first folder regards the calculated mass flow rate of all the branches,
- The second and third are respectively the supply pressure and the return pressure of all the nodes of the network,
- The third and the fourth are associated, instead, to the supply and return temperatures of all the nodes,
- There is also a LogFile.txt file produced by *NeMo* and filled in with the description of the pre-processing start time, the end-simulation time, and the elapsed time [s].

All the output, as of the input, are based on the same supply input time-step.



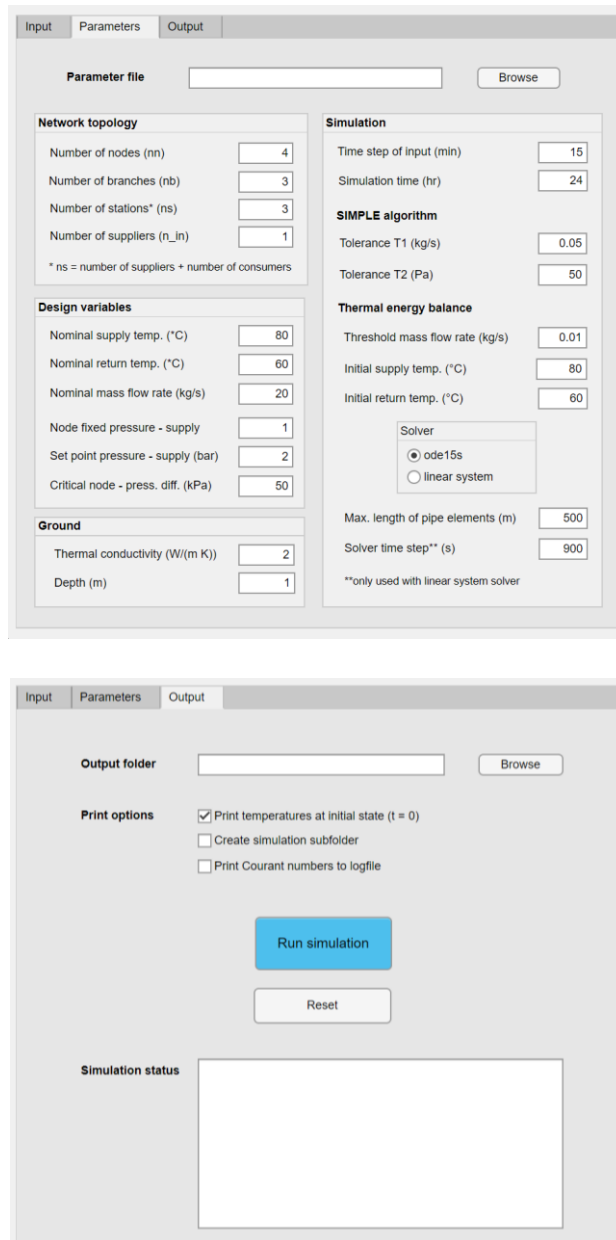


Figure 2.3: NeMo interface MATLAB App: a) Input, b) Parameters, c) Output.

2.2 Detailed Model

The Detailed Model²⁴, explained in this paragraph, was developed within the LIFE4HeatRecovery project. It is coded in Octave (preserving compatibility with MATLAB), and it describes the hydraulic and thermal dynamics of the network, as well as *NeMo*. The network geometry is implemented as a graph, with vertices positioned according to Figure. The hydraulic boundary conditions are provided

by flow rates at user vertices (that are calculated from the user load profiles assuming a constant supply return temperature difference of 5°C, controlled by regulating valves at HP substations) and by the pressure at a reference vertex. The thermal boundary conditions are provided by source temperatures. The hydraulic part is solved independently from the thermal part by using the Kirchhoff laws at network nodes. The relation between the pressure losses Δp and flow rate \dot{V} is assumed to be of the type:

$$\Delta p \propto \dot{V}^n \quad (2.18)$$

while pump control basically assumes a fixed pressure difference. The solution of the thermal part depends instead on the hydraulic solution, as it uses a one-dimensional heat transfer equation which depends on velocity (and neglects thermal diffusion):

$$(\partial_t + v\partial_x) T_f = -\frac{T_f - T_g}{\tau} \quad (2.19)$$

where:

- T_f is the fluid temperature,
- T_g is the ground temperature around the pipes
- v is the fluid velocity,
- τ is the time constant.

The latter is related to the overall pipe heat loss coefficient U_{avg} by:

$$\tau = \frac{\rho c_p \pi \left(\frac{D}{2}\right)^2}{U_{avg}} \quad (2.20)$$

where:

- D is the pipe diameter,
- ρ is the water density,
- c_p is the water specific heat.

For the case of constant ground temperature, solution of (2.19) can be written as:

$$T_f(t, x) = T_g + [T_f(t_0, x - \int_{t_0}^t v(t') dt') - T_g] e^{-(t-t_0)/\tau}$$

(2 . 21)

Where t_0 is the initial time. Exploiting this semi-analytical solution, the outlet temperature of a pipe section can be calculated as function of the inlet temperature at previous times.

The solution could be generalized to non-constant ground temperature; however, this effect was neglected since the time-scale for its variation is much longer than that for the network operation. With this assumption, the validity of solution (2.21) can be checked by explicitly carrying out the time and space derivatives.

Input, Output

The Detailed Model doesn't have a developed interface App as *NeMo*, every input are inserted in the main Octave code of the models as .txt files, differently from the Excel files exploited by the other model.

The main inputs of the detailed model are basically similar to the ones implemented in *NeMo*:

- Hourly load profile for each single user,
- Average ambient temperature profile,
- Source temperature,
- User temperatures,
- HP performance,
- Topology of the network.

And the model main outputs provide:

- HP electricity consumption,
- Thermal energy delivered by the network (on the evaporator side of HPs),
- Thermal losses,
- Pumping consumptions,
- CO₂ emissions.

The output of the Detailed Model can be derived in *NeMo* using the output folder of mass flow in branches, supply and return pressure (for the pumping

consumption), supply and return temperature (for thermal losses), except for the latter output CO₂ emissions.

Chapter 3

Case study

3.1 Ideal simplified case study

The ideal simplified case study, introduced in this chapter, is inspired to the one examined by UniPD taken from the literature²⁵.

The aim of this part is to evaluate the accuracy and the differences between the different simulation tools examined, NeMo and Detailed Model by Eurac.

It consists of three single pre-insulated pipes connecting four nodes, which first of them is the supply station and the latter one is the consumers, the remaining middle nodes have the task to connect the vertices.

It is assumed an ideal square wave on temperature that propagates through the edges. The inlet temperature is 30°C in the first 40 minutes, 50°C for the next 40 minutes and finally drops again to 30°C and remains constant for the last 100 minutes. The most important characteristics of pipes, ground, temperature, and the simulation parameters are presented in the subsequent table 3.1:

Parameters	Value	Units
Total network length	500	m
Internal diameter of the pipe	80	mm
External diameter of the pipe	83	mm
Diameter of casing	150	mm
Thermal conductivity of insulation	0.033	W/(m K)
Thermal conductivity of the ground	2	W/(m K)
Depth	1	m
Undisturbed ground temperature	8	°C
Initial temperature at inlet node	30	°C
Initial temperature at outlet node	30	°C
Mass flow rate	2.74	kg/s
Input time-step	5	min
Simulation time	3	h
Heat load	3	kW

Table 3.1: Characteristics of the ideal simplified case study.

The inlet temperature and the water mass flow rate of the supply pipe are set as boundary conditions and the goal is to compare the resulting outlet temperature profile of *NeMo* and *Detailed Model* with the theoretical solution, implemented in MATLAB and discussed in the following chapter 4: *Methodology*.

As the mass flow rate is fixed as a boundary condition, the velocity of the fluid inside the conduits is constant, and it can be calculated as:

$$v = \frac{\dot{m}}{\rho_w \pi \left(\frac{D_{int}}{2}\right)^2} = 0.5451 \frac{m}{s} \quad (3.1)$$

3.2 Real case study - Aalborg DHN

The real case study examined in this work is part of the Aalborg district heating network, in particular, the focus is on the Aalborg University Campus. This network is included in the traditional 3rd generation DHN category, indeed the supply temperature is about 85-90°C, instead of 50-60°C presented in 4th generation DHN.

It consists of 158 nodes connected by 157 branches, with different characteristics of thermal insulation, diameters and length. The supply temperature varies every days in order to follow a climatic curve related to the outdoor temperature and discussed in the paragraph 4.2.1.

The main supply station (node 8) is a cement factory located in the north of the grid, but other supply stations such as Data Centre dislocated around the pipes can be exploited to provide waste heat sources for the network.

The geometry of the DHN, reported in the next figure, is provided by Aalborg Forsyning by means of a QGIS shapefile in which it were attached the network coordinates, topology, and some performing data such as thermal power, supply temperature, return temperature of the substation.

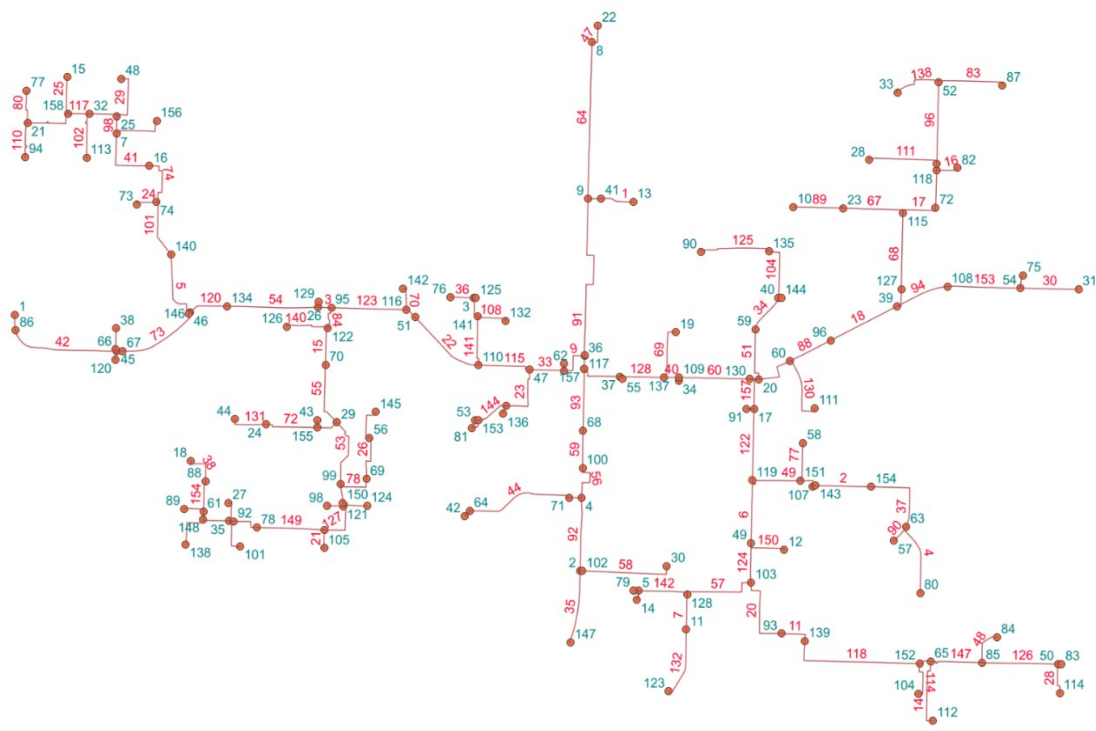


Figure 3.1: Aalborg DHN.

Chapter 4

Methodology

4.1 Ideal simplified case study

The theoretical outlet temperature profile of the heat carrier fluid has been determined by means of MATLAB and the characteristics explained in the table 3.1.

The process to obtain that profile started from the one-dimensional heat equation for a constant cross-section, written neglecting the diffusion term, as for the thermal balance of *NeMo* and *Detailed Model*.

The equation, expressing the thermal power per unit volume, results:

$$\rho c_p (\partial_t + v \partial_x) T = -a(T - T_{ext}) \quad (4.1)$$

Where:

- v is the fluid velocity,
- T is the fluid temperature,
- ρ is the fluid density ($\rho_w = 997 \text{ kg/m}^3$),
- c_p is the fluid specific heat ($c_p = 4187 \text{ J/kg K}$),
- T_{ext} is the surrounding temperature ($T_{ground} = 8^\circ\text{C}$),
- a has the dimensions of a heat exchange coefficient divided by length.

Dividing both sides by ρc_p and defining the time constant $\tau = \rho c_p / a$, the equation becomes the following:

$$(\partial_t + v \partial_x) T = -(T - T_{ext}) / \tau \quad (4.2)$$

All the variables, except for the latter one τ , are assumed to be time dependent. Moreover, the fluid temperature T is clearly space-dependent due to the thermal losses along the pipe, instead, T_{ext} is assumed to be constant in space; finally, v cannot be space-dependent, because of the constant cross section and the incompressibility of the water.

The thermal power across a thermal resistance R_{th} for a certain temperature difference ΔT is given by $P_{th} = \Delta T/R_{th}$, related to Fourier law.

The thermal resistance R_{th} [K/W] related to i -th annulus of a set concentric pipes can be calculated by means of internal diameter D_i [m], thermal conductivity k_i [W/m K], and length L :

$$R_{th,i} = \frac{\ln\left(\frac{D_{i+1}}{D_i}\right)}{2\pi L k_i} \quad (4.3)$$

For multiple concentric pipes, the total thermal resistance could be obtained as the sum of i -th annulus ones: $R_{th,tot} = \sum_i R_{th,i}$.

In this case study, the pre-insulated pipes examined is composed in order by:

- An annulus of steel ($k = 50 \text{ W/m K}$) that embodies the fluid shell,
- An annulus of PU ($k = 0.033 \text{ W/m K}$) that represents the insulation,
- An annulus of PE ($k = 0.38 \text{ W/m K}$) becoming the splitter from the ground.

As mentioned previously, a has the dimensions of a heat exchange coefficient divided by length, as well as an inverse thermal resistance per unit volume. Neglecting the heat transfer coefficient between the fluid and the pipe walls, the coefficient a can be derived from the overall resistance and the overall fluid volume as $a = 1/(V R_{th})$, where $V = L \pi \left(\frac{D}{2}\right)^2$ and $D = D_i$ is the inner diameter.

This case study comprises constant value of velocity and external temperature; in the absence of sources and sinks, the Equation (2) becomes $(\partial_t + v\partial_x)T = 0$, so any function $f(x - vt)$ is a solution.

Defining $\Theta(t, x) = T(t, x) - T_{ext}$, obtaining:

$$(\partial_t + v\partial_x)\Theta = -\Theta/\tau \quad (4.4)$$

With the change of coordinates (corresponding to a change of reference frame) $\tilde{t} = t$, $\tilde{x} = x - vt$, this equation becomes:

$$\partial_{\tilde{t}}\Theta = -\Theta/\tau \quad (4.5)$$

which is readily solved as $\Theta(\tilde{t}, \tilde{x}) = f(\tilde{x})e^{-\tilde{t}/\tau}$, i.e., $T(t, x) = T_{ext} + f(x - vt)e^{-t/\tau}$, where f is some function which can be found from the initial conditions known at the time $t = 0$, namely $f(x) = T(0, x) - T_{ext}$. The solution as a function of the initial conditions can hence be expressed as:

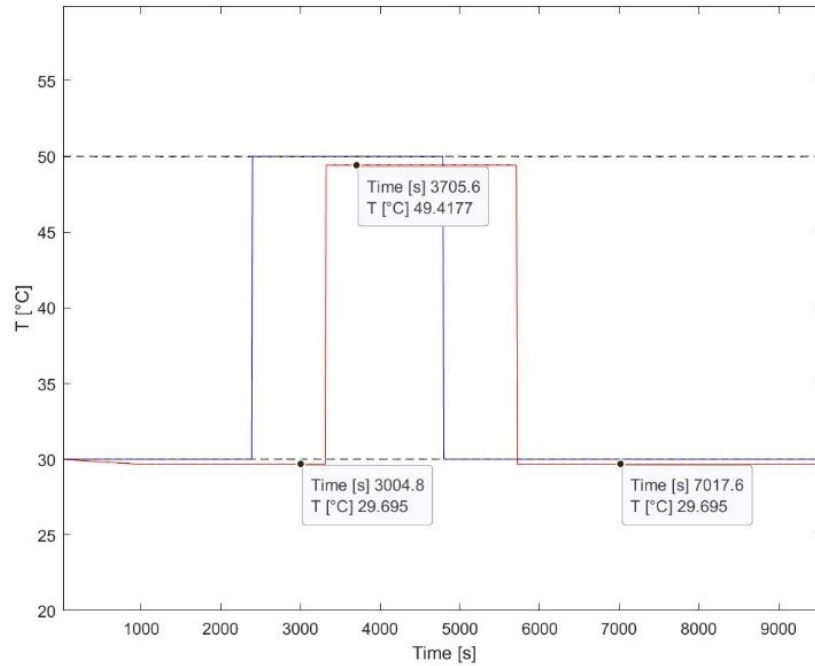
$$T(t, x) = T_{ext} + [T(0, x - vt) - T_{ext}]e^{-t/\tau} \quad (4.6)$$

For a finite system, besides initial conditions (boundary conditions in time) one also needs to fix inlet conditions (boundary condition in space). Assuming inlet conditions are fixed at $x = 0$, one cannot calculate $x - vt$ for the times larger than $\Delta t_b = x/v$, which is the time needed to reach the boundary. For such times, the solution can instead be expressed as a function of the inlet conditions as:

$$T(t, x) = T_{ext} + [T(t - \Delta t_b, 0) - T_{ext}]e^{-t/\tau} \quad (4.7)$$

In this case study, $\Delta t_b = L/v = 917.26$ s; $T(x, t)$ represents a composition of the two-equation mentioned above for different t values (for $t < \Delta t_b$ (4.6) works, on the flip side, (4.7) represents the optimal equation).

The results of the theoretical solution are presented in the following plots:



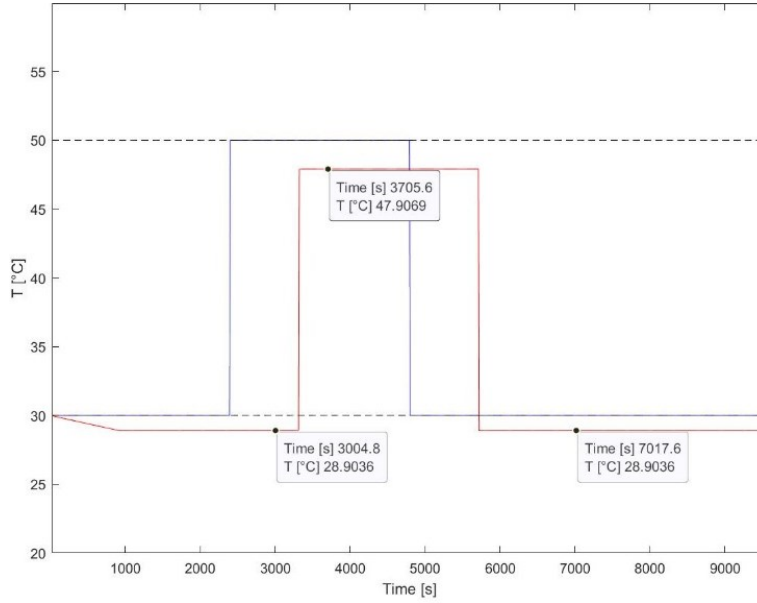


Figure 4.1: : Theoretical solution with a) 35 mm thickness, b) 5 mm thickness.

The blue line represents the inlet temperature profile set as an input, the red one corresponds to the outlet temperature profile of the fluid.

The step function of the inlet and outlet temperature clearly concern with input boundary conditions, but T_{out} profile is shifted to lower values of temperature due to the thermal losses propagates along the pipes, because of the smaller value of the ground temperature ($T_g = 8^\circ C$), compared to the fluid one ($30^\circ C$, $50^\circ C$, $30^\circ C$).

The effect of the thermal losses is the only one accused by the pipes, because the term regarding the thermal diffusion between fluid and wall is neglected, as revealed in (2.13).

With these characteristics of the pipes and the ground, the resulting outlet temperature obtained from the theoretical solution after three hours simulation is about $29.69^\circ C$ when the inlet temperature is $30^\circ C$, and $49.42^\circ C$ when it is $50^\circ C$ as indicated in Fig. 4.1a.

The delay time between the two curves deals with the velocity of the fluid, and it can be determined as:

$$\tau_{delay} = \frac{L}{v} = 917.26 \text{ s}$$

(4 . 8)

After τ_{delay} , the outlet profile starts to appear because of the fluid signal arrives at the end of the edges.

An interesting observation could be done changing the thickness of the pipes from 35 mm to 5 mm, and the effects are shown in Figure 4.1b.

The different situation among the two pictures has to do with the thermal losses: reducing the thickness of the pipes seems to replace the pre-insulated ones with non-insulated ducts. The consequence of this effect produces the decrease of the outlet fluid temperature to 28.90°C when the inlet temperature is 30°C, and 47.91°C when it is 50°C, because of the higher heat exchange with the ground.

The amount of heat losses [kW] can be derived as:

$$q_{losses} = \dot{m} c_{p,w} (T_{inlet} - T_{out}) \quad (4.9)$$

Inlet temperature [°C]	Heat losses - 1 st case [kW]	Heat losses - 2 nd case [kW]
30	3.55	12.50
50	6.76	23.97

Table 4.1: Amount of heat losses [kW] for different inlet temperature.

The heat losses in the 2nd case are approximately four times higher compared to the 1st case.

Furthermore, as the velocity is constant, the delay between inlet and outlet profile temperature is keeping equal. Modifying the velocity value, the delay of the system will be influenced in order with (4.8).

4.1.1 *NeMo*

The ideal study case is represented by a set of nodes and oriented branches, and the adjacency matrix determines their mutual connections. Once the geometry is established, the pressure and temperature outlet profiles are calculated.

NeMo needs five different types of input Excel files, as explained in 2.1.3:

- Loads:

Input time-step	Heat loads [kW]	Mass flow rate [kg/s]
1	3	2.74
2	3	2.74
...	3	2.74
36	3	2.74

Table 4.2: Definition of Loads.xlsx input file.

- Substations:

Prosumer	Node ID	Prosumer type
Supply station 1	1	Supplier
Consumer 1	4	Consumer

Table 4.3: Definition of Subs.xlsx input file.

- Network:

Branch ID	Upstream node	Downstream node
1	1	2
2	2	3
3	3	4

	L	D_i	\dot{m}_{nom}	Roughness	D_{ext}	D_{ins}	k_{ins}	Q_{v1}	dP_1	Q_{v2}	dP_2	η_{pump}
1	100	0.08	5	0.05	0.083	0.093	0.033	1	1.0	6	6.0	0.9
2	300	0.08	5	0.05	0.083	0.093	0.033					
3	100	0.08	5	0.05	0.083	0.093	0.033					

Table 4.4: a) Incidence Matrix, b) Characteristics of the pipes.

- Ground:

Input time-step	T _{ground} [°C]
1	8
2	8
...	8
36	8

Table 4.5: Definition of Ground.xlsx input file.

- Parameters:

Input time-step	5 min
Simulation time	3 hours
Tolerance T1	0.0001 kg/s
Tolerance T2	50 bar

Table 4.6: Definition of the Parameters.xlsx input file.

In the current version of the model *NeMo*, the user is free to choose the resolution method for the transient heat propagation problem between the first-order ordinary differential equation solver (ODE) and the linear system (LS) solver. The latter requires the user to set the internal calculation time-step $\Delta\tau$, otherwise, using ODE solver, the time-step is decided by *NeMo*.

Once that all the input files have been filled, *NeMo* provides the results related to the input time-step decided by the users (in this case, 5 min. for 3 hours), the step-size and the internal calculation time-step.

The precision of the model examined in the chapter ... is based on the Courant number, a dimensionless number that expresses the ratio between the physical velocity v (velocity of the water stream in each pipe element) and the ‘velocity of calculation’, i.e., the ratio between the length of each element Δx and the time-step $\Delta\tau$ used by the numerical method to update the temperature distribution.

$$Co = \frac{v \Delta\tau}{\Delta x}$$

(4 . 10)

The Courant number indicates how fast the temperature information travels on the computational grid; it is regarded as the most important parameter as far as the performance of numerical methods for convective flow is concerned.

A necessary condition for the stability is $Co < 1$: the step size must be smaller than the time interval it takes for the flow to cross the small distance between two adjacent points.

Fig. 4.2 shows the outlet temperature of the step wave for the model, the results have been obtained with a fix value of $Co = 0.8$, changing the step size Δx and the time interval $\Delta \tau$.

It can be noticed that increase the number of discretize elements of pipe (i.e., reducing the step size and consequently the calculation time-step) reduces the artificial diffusion and leads to a better approximation of the theoretical wave, as it can be seen for the Linear Solver resolution system with $\Delta x = 10\text{ m}$, $\Delta \tau = 15\text{ s}$ represented by the purple line, instead of the ODE solver represented by the green one.

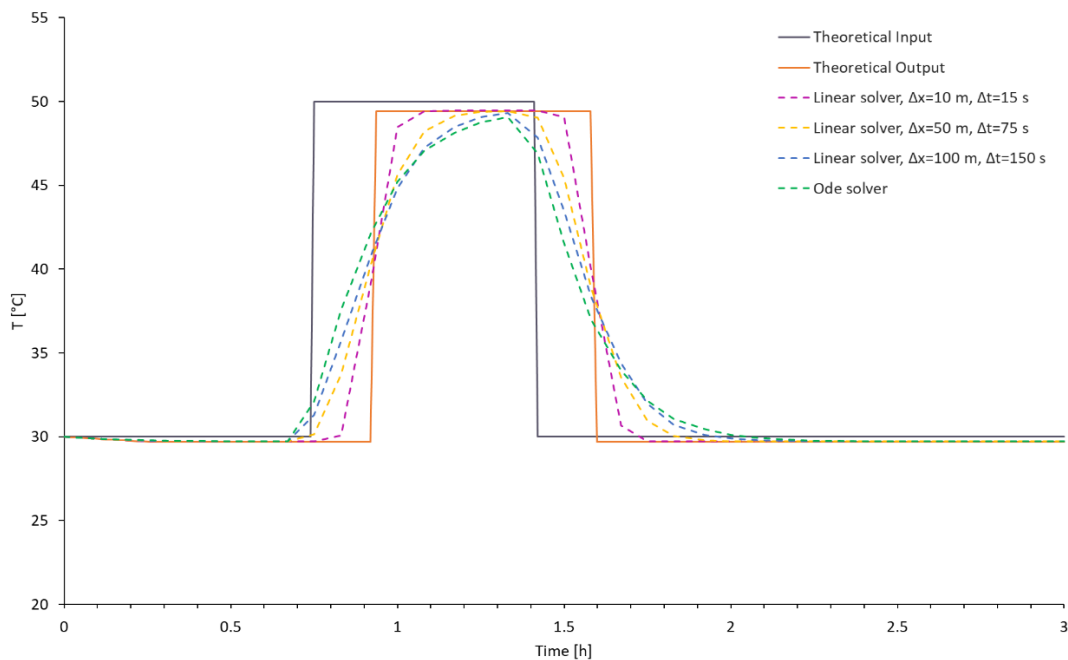


Figure 4.2: NeMo outlet temperature profiles for $Co=0.8$ fix.

As revealed in the previous figure, the precision of the output results doesn't deal directly with Co , because with a constant value of the Courant number, different plots have been found. This is reasonable because same Co number with 5-times

lower time-step implies solving the equation 5 times more, i.e., having a finer mesh in space and time.

For a given Courant number, the temperature profiles obtained with lower Δx give a lower error (in wave start and in width, that is clear from the plot) than those obtained with higher Δx .

The most important thing to highlights is the influence of the calculation time-step $\Delta\tau$ or the step size Δx , Fig. 4.3, where the most accurate results are provided by linear solver, $\Delta x = 10\text{ m}, \Delta\tau = 15\text{ s}$ because of the smaller value of Δx .

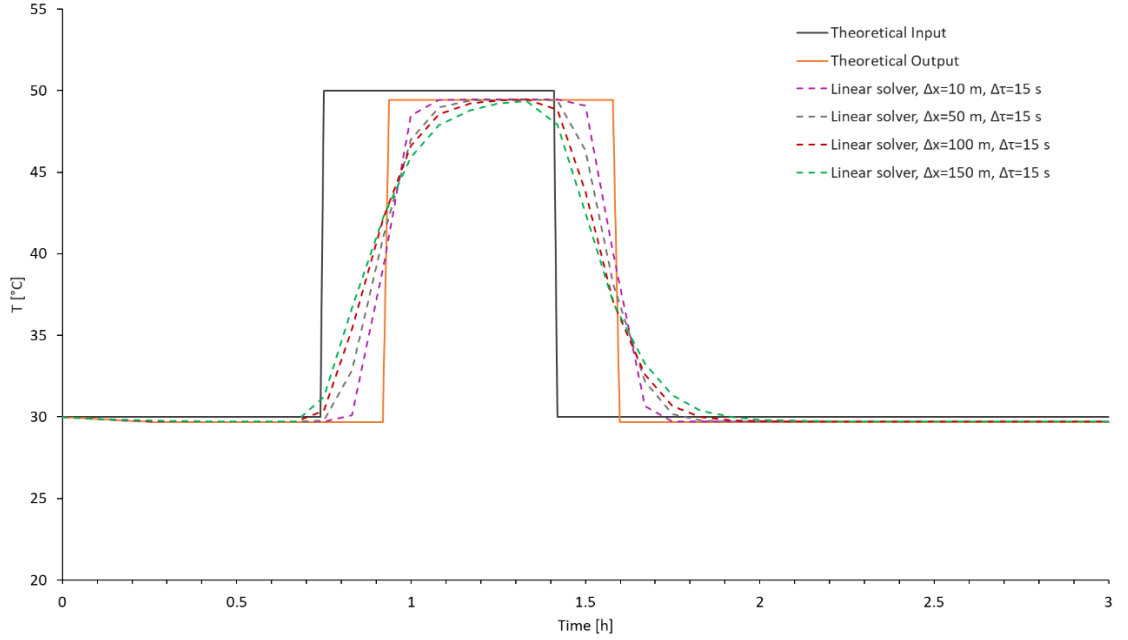


Figure 4.3: NeMo outlet temperature profiles for $\Delta\tau=15\text{ s}$ fix.

4.1.2 Detailed Model

The input of this Octave-based model are similar to *NeMo* ones, without an uploading phase using a developed App interface. Detailed Model read the input file as .txt by means of instructions in the Octave code.

As *NeMo* is related to the Courant number, the step-size, and the time-step of the simulation to evaluate the accuracy of the results, the Detailed Model is connected to other parameters expressed in the successive formula:

$$\Delta L = v \Delta t$$

(4 . 11)

Where:

- v is the velocity of the fluid's particles,
- Δt is the time-step of the simulation, same as $\Delta \tau$ for *NeMo*.

ΔL is the space cover by the particles during at a certain velocity and during the consider time-step of simulation.

It can be possible to derive from ΔL an important parameters for the simulations of this model as the maximum number of particles in the duct:

$$n_{max\ particles} = \frac{L}{\Delta L}$$

(4 . 12)

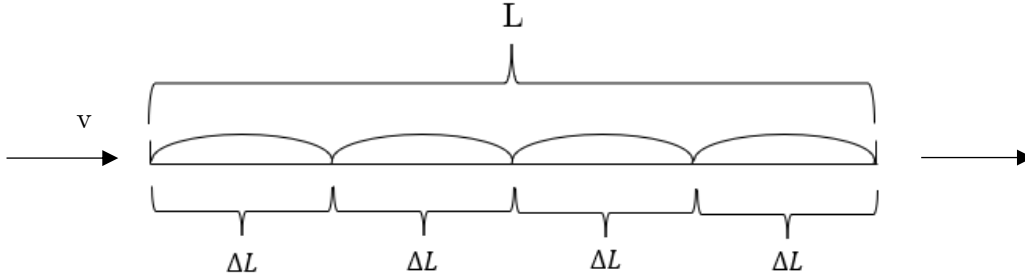


Figure 4.4: Definition of the Detailed Model new parameter ΔL .

The maximum number of particles in this case is the measure of the results precision, related to the velocity of the fluid and the time-step of simulation. Choosing a maximum number of particles higher than the calculated $n_{max\ particles}$ the accuracy doesn't improve, or better, the improving is inappreciable, as demonstrated in the next figure:

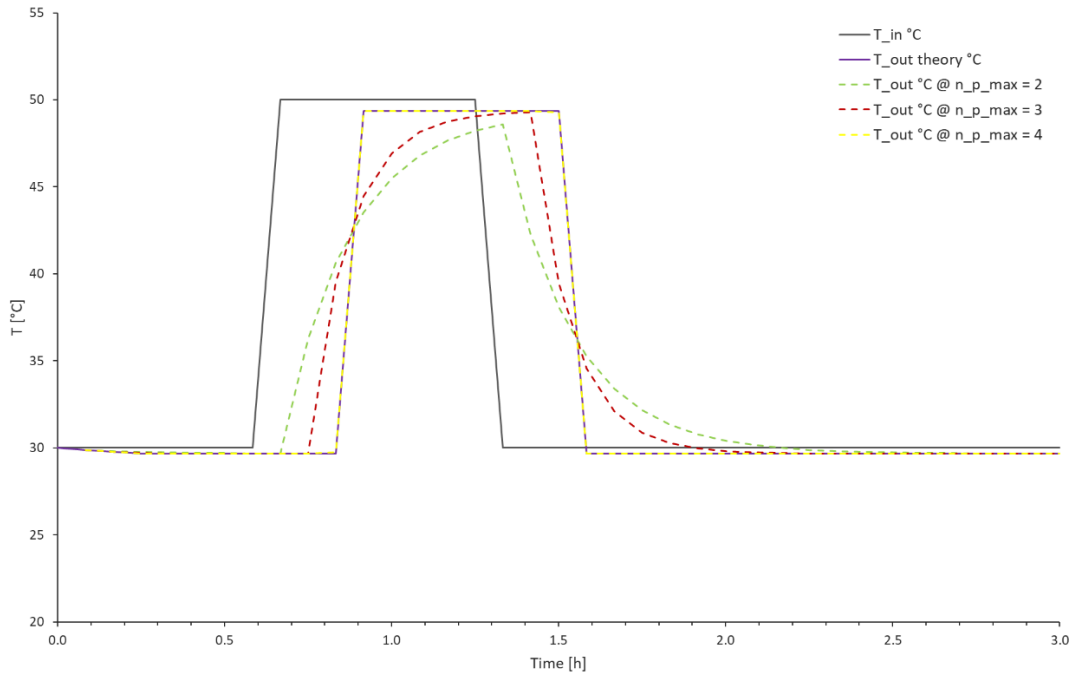


Figure 4.5: Detailed Model outlet temperature profiles for different value of max $n_{particles}$.

In Figure 4.5 it is shown the accuracy of the results according with the maximum number of particles. In this ideal case, the resulting n_p_max is equal to four particles. The process of precision improvement is related to the profile described in the plot.

Exploiting the calculated maximum number of particles, the profile is substantially overlapped to the theoretical one, there isn't a highlighted difference between yellow curve and the purple one.

The user can choose a higher value of n_p compared to the calculated one (4, in this case), but the refinement compared to the calculated value is not appreciable.

To modify the calculated value of number of particles in order to obtain a better accuracy, it is necessary to lower the velocity of the fragments of fluid, indeed the space cover is reduced, and the consequence is the increasing of $n_{max\ particles}$ that run in the duct, on which is based the precision of the model.

4.2 Real case study: Aalborg DHN

The necessary part that precede this analysis is represented by the monitoring data of the Aalborg DHN, useful to fill in the input files of *NeMo*. Inside the project LIFE4HeatRecovery the monitoring data will be provided by Aalborg Forsyning, but for this work it has been decided to reproduce the thermal profile of the nodes by means of *EUReCA* software, developed by UniPD.

4.2.1 *NeMo* inputs

EUReCA: Energy Urban Capacitance Approach

The Energy Urban Capacitance Approach – *EUReCA*²⁶ - is a stand-alone Python-based Urban Building Energy Modelling tool. The software aims at the bottom-up simulation of large districts and cities, predicting the hourly building heating and cooling demand and consumptions in an efficient and reliable way. Simulation is carried out by means of semantic geo-referenced district data that includes information about buildings' age-class and end-use. The construction year is used to associate to each building a specific set of construction typologies, i.e., roof, external wall, ground floor, etc., named buildings envelope archetype. An integrated database includes several building archetypes with structures' thermal parameters corresponding to the age classes. Another additional database provides the miscellaneous operational schedules and gains for different end-uses, in a similar approach. This research project has been developed within the BETALAB research group of the University of Padua.

The thermal behaviour of buildings is then modelled by means of two possible simplified dynamic models, both based on the electrical analogy:

- a single capacitance thermal network,
- a two capacitances thermal network, respectively from ISO 13790 and VDI 6007 Standards.

EUReCA can handle CityJSON models to build up the city, which are inherently 3D, and 2D GeoJSON models derived from importing and reconstructing building geometries from ESRI Shapefiles by means of manipulating JSON data through the Python environment.

In this work, surfaces and vertices are imported by the following workflow:

- GeoJSON: the building is created by combining footprint's vertices and building-height attribute, which must be included in the input file. The surfaces are generated considering an extrusion of the polygon as equal to the building height. Even in this case, surfaces are created by means of the *surface* class, enabling the calculation of area and orientation.

For all the Aalborg buildings served by the DHN, 2D GeoJSON file has been built up with a QGIS project.

QGIS is a free and open-source cross platform desktop geographic information system (GIS) application that supports viewing, editing, printing, analysis of geospatial data, and exporting graphical maps. QGIS supports raster, vector, and mesh layers. Vector data is stored as either point, line, or polygon features.

Description of the Aalborg buildings

The Aalborg DHN examined in this work is only the section around the Aalborg University Campus of a wider extended network and is made up of 271 buildings. The area extends for about 2 km² and includes different type of end-uses buildings:

- 163 residential buildings, 60.1%,
- 20 offices, 7.4%,
- 82 service buildings (mainly university structures), 30.3%,
- 6 commercial buildings, 2.2%.

The complex of structures explained above is represented in the following figure, with the buildings', the nodes, and the pipes layer:

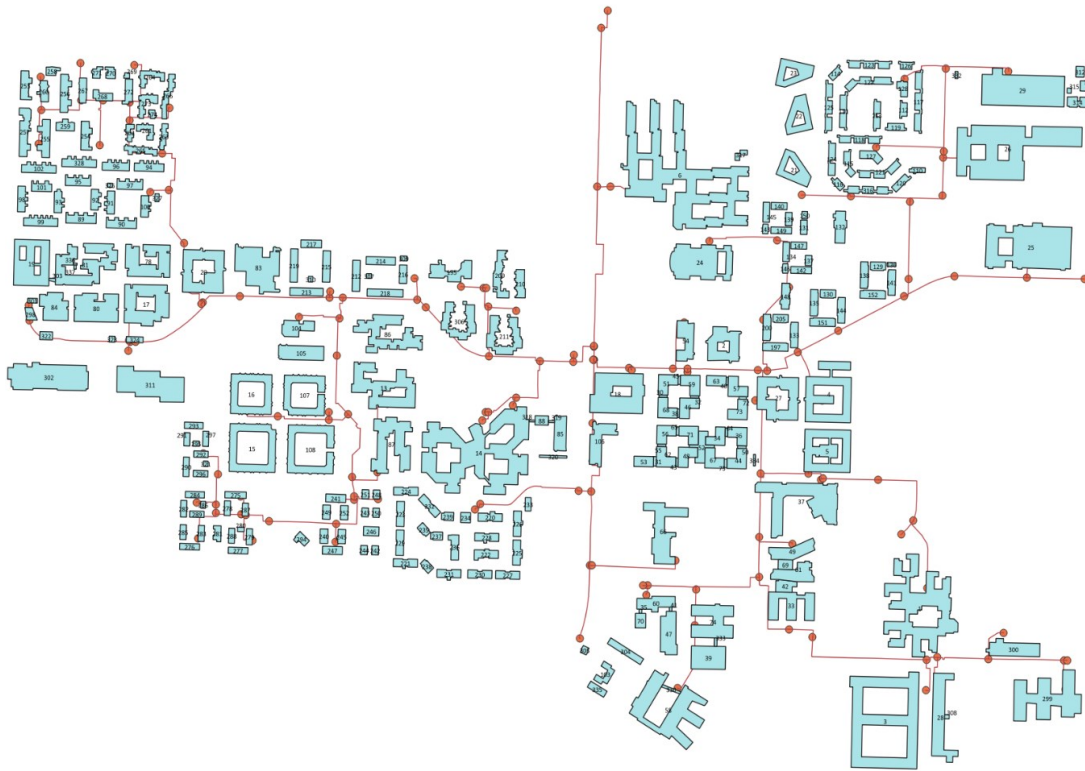


Figure 4.6: QGIS buildings, nodes, pipes layer.

First, to assign the right labels of age-class, end-uses, and number of floors for all the constructions, a work of mapping using Google Maps was necessary, checking every single building served by the DHN. Due to difficulties in deducting the age of the buildings by Google Maps, it has been assumed a year built for most of the buildings around 1995, because of the quality of external surface.

The chosen age-classes envelope archetype comprises:

- Roof: Ceiling with reinforced brick-concrete slab (24 cm),
- External wall: Hollow/solid bricks with insulated cavity,
- Ground floor: Floor with reinforced concrete slab, lightweight screed (12 cm),
- Internal ceiling: Internal floor with reinforced brick-concrete slab (24 cm), traditional screed (12 cm), insulation (2 cm),
- Internal wall: Hollow tiles and plasters (8 cm),
- Windows: Double glazing, air filled, metal frame with thermal break (transmittance $U = 3.4 \text{ W/m}^2 \text{ K}$).

Afterwards these labels had to be added inside the attribute table of the layer ‘AalborgBuildings’, in order to modify the GeoJSON related to the constructions, which will be required for *EURCA* input.

Moreover, the geo-referenced description of the district has been built with this other following characteristics inside the attribute table of the layers previously appointed:

- Building ID,
- Name,
- Height,
- Number of floors,
- External wall coefficient,
- Volume Coefficient,
- Cooling plant name,
- Heating plant name.

The height of the buildings is calculated as the product between the height of a single floor (3.2 m), and the number of floors derived by the Google Maps.

The buildings height and number of floors allow the calculation of the heated volume and the external walls area by extrusion of the footprint, as expressed previously. End-use and age-class labels associate buildings to a particular operational schedule and envelope archetype, respectively. The two geometrical coefficients are distinct multipliers of the heated volume, and the external wall area. The external wall area and heated volume of each building has been corrected to the real values by means of these two. These geometrical corrections are proposed to stress the impact of geometric data in the calculation of heat load due to multiple geometrical approximations, cause mainly by extrusion.

Beyond the labels explained above to adjust the geoJSON model, there are several other input to prepare for *EURCA*, that permits to simulate the energy consumption:

- A *weather_data.epw*, that is the climatic file of Aalborg, downloaded from the Danish Meteorological Institute (DMI) through an Application Programming Interface (API) for the year 2021.

The climatic file must be as precise as possible, because it may affect significantly the final hourly consumption, influencing the cooling load for the buildings,

- A *Envelopes.xlsx* spreadsheet. It includes the thermophysical properties of building envelopes defining different archetypes related to age-class,
- A *Schedules.xlsx* spreadsheet. It includes the operational schedules of occupancy, appliances, temperature, humidity setpoints, HVAC usage for different end-uses. For this case study, the plant availability of the residential buildings and commercials is set to the value 1, because of the presence of people in the weekend, the power plant can turn on if the indoor temperature is lower than the setpoint temperature. Moreover, the residential buildings is the only one where the ventilation rate is considered zero due to the lack of mechanical ventilation system as assumption. In the other type of buildings, i.e., office, service, the plant availability in the weekend is set to 0, because of the absence of people inside. There are two possible ways to set up the end-uses usage: using the daily mode or the yearly mode,
- A *PlantList.xlsx* spreadsheet. The file includes the input data of many plants model, for different sizes,
- The *SimInput* file, which defines the simulations parameters,
- The *GeoJSON* model, to reproduce the building of the case study, with the right labels on the attributes table.

In the following tables are presented the input values of the *Schedules.xlsx* spreadsheet, for every type of buildings, during the week (Table 4.7), and the weekend (Table 4.8). All of them with the same end-uses has the same values of input despite, the schedules can be different between several residential, offices, services structures, or commercials each other.

HeatSP is the setpoint temperature [°C] of the heating plant, Vent_FlowRate is the ventilation flow rate [m³/s m²] that air handling unit provides, Availability (AVL) is a choose between value 1, when the plant is switched on, and value 0 when it is switched off.

	Residential		Offices		Services		Commercials	
	<i>HeatSP</i>	<i>Vent_Flow Rate</i>	<i>Heat SP</i>	<i>Vent_Flow Rate</i>	<i>Heat SP</i>	<i>Vent_Flow Rate</i>	<i>Heat SP</i>	<i>Vent_Flow Rate</i>
<i>AVL</i>	1	0	1	1	1	1	1	1
Hours								
1:00	20	-	14	0	14	0	14	0
2:00	20	-	14	0	14	0	14	0
3:00	20	-	14	0	14	0	14	0
4:00	20	-	14	0	14	0	14	0

5:00	20	-	14	0	14	0	14	0
6:00	20	-	17	0	17	0	17	0
7:00	20	-	17	0	17	0	17	0
8:00	20	-	19	0.0008	19	0.0038	19	0.0021
9:00	20	-	20	0.0008	20	0.0038	20	0.0021
10:00	20	-	20	0.0008	20	0.0038	20	0.0021
11:00	20	-	20	0.0008	20	0.0038	20	0.0021
12:00	20	-	20	0.0008	20	0.0038	20	0.0021
13:00	20	-	20	0.0008	20	0.0038	20	0.0021
14:00	20	-	20	0.0008	20	0.0038	20	0.0021
15:00	20	-	20	0.0008	20	0.0038	20	0.0021
16:00	20	-	20	0.0008	20	0.0038	20	0.0021
17:00	20	-	20	0.0008	20	0.0038	20	0.0021
18:00	20	-	20	0.0008	20	0.0038	20	0.0021
19:00	20	-	14	0	14	0	20	0.0021
20:00	20	-	14	0	14	0	20	0.0021
21:00	20	-	14	0	14	0	20	0.0021
22:00	20	-	14	0	14	0	14	0
23:00	20	-	14	0	14	0	14	0
0:00	20	-	14	0	14	0	14	0

Table 4.7: Different week schedules for type of buildings.

	Residential		Offices		Services		Commercials	
	<i>Heat</i> <i>SP</i>	<i>Vent_Flow</i> <i>Rate</i>	<i>Heat</i> <i>SP</i>	<i>Vent_Flow</i> <i>Rate</i>	<i>Heat</i> <i>SP</i>	<i>Vent_Flow</i> <i>Rate</i>	<i>Heat</i> <i>SP</i>	<i>Vent_Flow</i> <i>Rate</i>
<i>AVL</i>	<i>1</i>	<i>0</i>	<i>0</i>	<i>0</i>	<i>0</i>	<i>0</i>	<i>1</i>	<i>1</i>
<i>Hour</i>								
1:00	20	-	-	-	-	-	14	0
2:00	20	-	-	-	-	-	14	0
3:00	20	-	-	-	-	-	14	0
4:00	20	-	-	-	-	-	14	0
5:00	20	-	-	-	-	-	14	0
6:00	20	-	-	-	-	-	17	0
7:00	20	-	-	-	-	-	17	0
8:00	20	-	-	-	-	-	19	0.0021
9:00	20	-	-	-	-	-	20	0.0021
10:00	20	-	-	-	-	-	20	0.0021
11:00	20	-	-	-	-	-	20	0.0021
12:00	20	-	-	-	-	-	20	0.0021
13:00	20	-	-	-	-	-	20	0.0021
14:00	20	-	-	-	-	-	20	0.0021
15:00	20	-	-	-	-	-	20	0.0021
16:00	20	-	-	-	-	-	20	0.0021

17:00	20	-	-	-	-	-	20	0.0021
18:00	20	-	-	-	-	-	20	0.0021
19:00	20	-	-	-	-	-	20	0.0021
20:00	20	-	-	-	-	-	20	0.0021
21:00	20	-	-	-	-	-	20	0.0021
22:00	20	-	-	-	-	-	14	0
23:00	20	-	-	-	-	-	14	0
0:00	20	-	-	-	-	-	14	0

Table 4.8: Different weekend schedules for type of buildings.

After the set-up of all input files, is possible to obtain the hourly consumption [kW] of the considered buildings as the sum of three folder output: *AHU*, *HeatFlow*, *LatentFlow*:

$$P_{th,i} = AHU_i + HeatFlow_i + LatentFlow_i$$

(4 . 13)

It's clear that the AHU, i.e., Air Handling Unit power, is equal to zero for every residential buildings, because of the assumption previously explained.

The power profile represented in Fig. 4.7 is referred to the week 52 of the year 2021, and it is affected by the outdoor temperature during the day; moreover, the daily profile in the week changes, in order to reach the higher peak in the first day, and lower peaks as days goes on. The reason can be found in the heat demand of buildings with absence of people during the weekend: the indoor temperature during this period slowly decrease, starting from the walls of the structures. In the first day of the week, the cooling load must also cover the declining of temperature disclosed in the weekend, so the power profile reveals the highest peak on Monday. As days goes on, the thermal capacitance of the walls keep the indoor temperature higher compared to the once in the weekend, so the cooling load slowly drop. For commercials and residential buildings this effect doesn't appear, as the power plant is always available (Fig. 4.8).

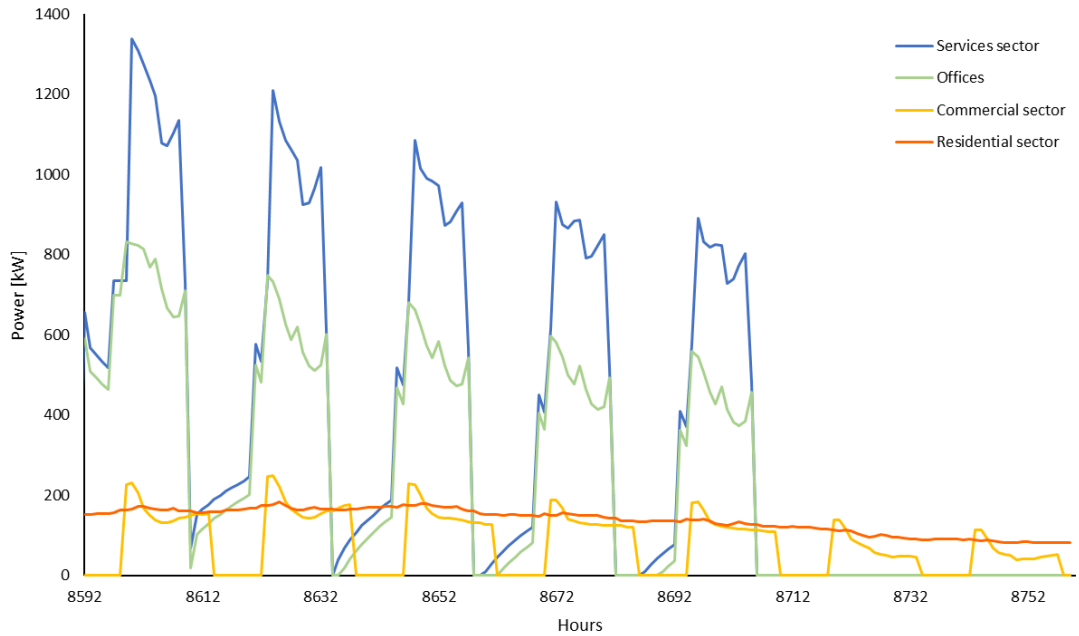


Figure 4.7: Thermal power profiles for diverse types of buildings.

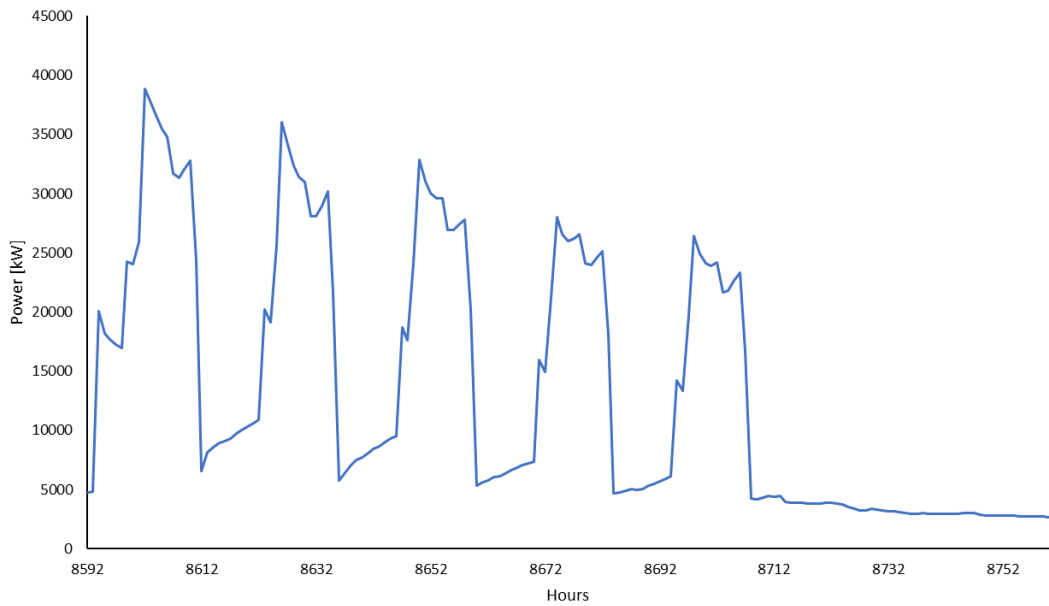


Figure 4.8: Maximum thermal power per hours for all the buildings.

Another important output folder is the *BuildingParams.xlsx*, a spreadsheet that contains the related parameters of the building such as the footprint, number of floors, total area, age, end-uses, height, transmittance of windows, roof, external wall, ground.

After calculating the power demand (kW), considering the linked area for every buildings, it is possible to evaluate the annual energy consumption [kWh/(m² year)] to verify the reality of the output results with the following equation:

$$\sum \frac{P_{th,i} \Delta t_i}{A_i}$$

(4 . 14)

Where:

- $P_{th,i}$ is the thermal power of a single building,
- Δt_i is the time step – 1h,
- A_i is the total area of the building, given by the product of the footprint and the number of floors.

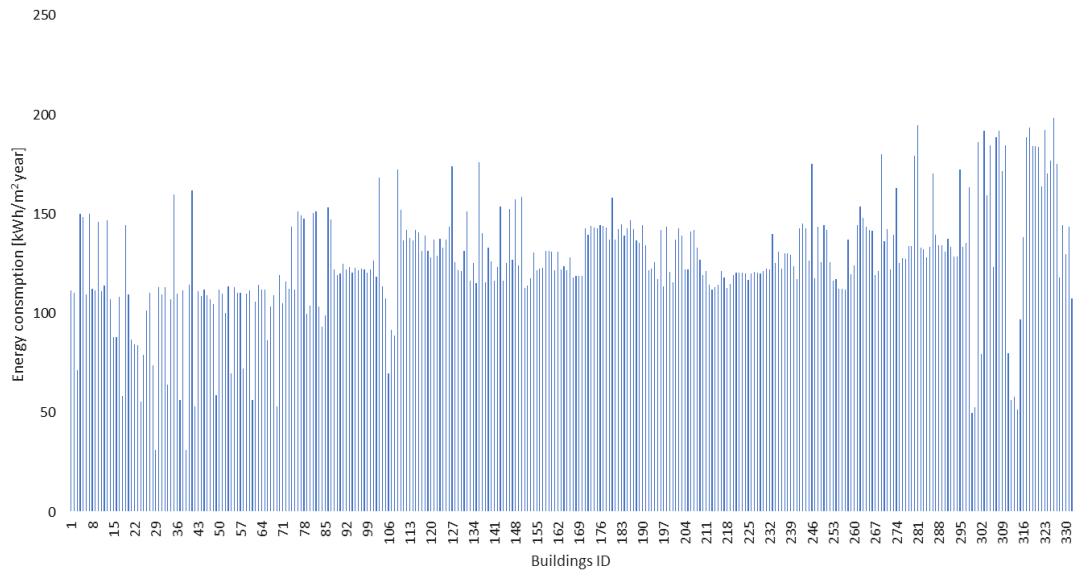


Figure 4.9: Annual energy consumption for every ID buildings.

As indicated in Fig. 4.9, the energy consumption of Aalborg buildings is higher than Italian standards, due to the lower outdoor temperature, thus average values of 130-140 kWh/(m² year) are usual. Furthermore, due to the significant number of non-residential buildings, the energy consumption is relevant because of the presence of AHU that increase the power demand.

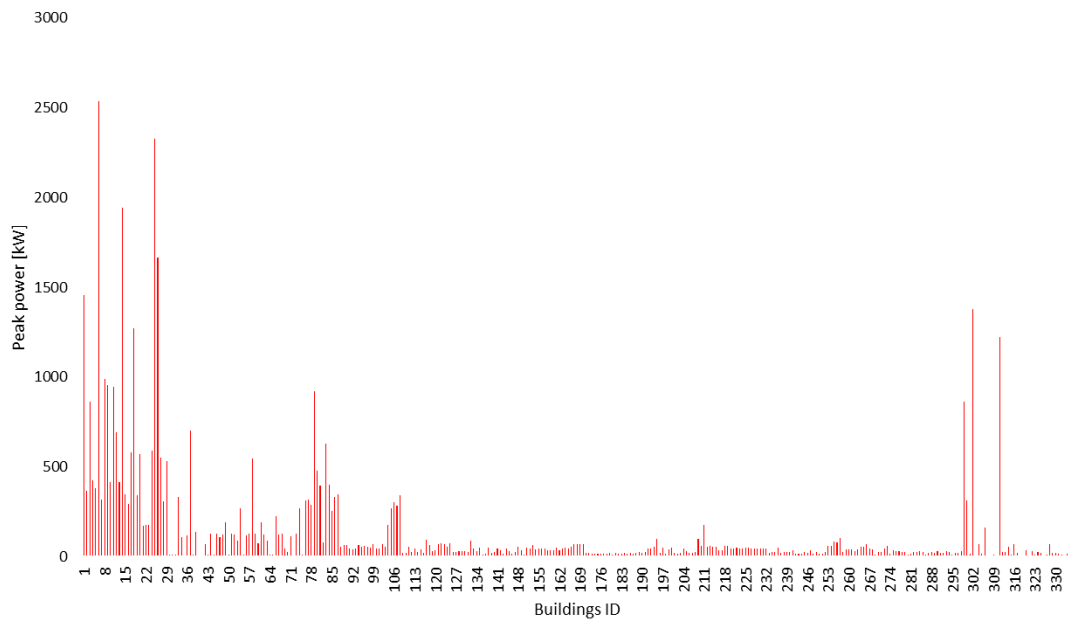


Figure 4.10: Thermal peak power for every ID buildings.

Related to Figure 4.10, some considerations can be mentioned:

- Running non-detailed simulation using basic parameters, as in this case, the estimates results are higher compared to detailed-model results that exploits more input like as the irradiance profile.
- Several buildings (non-residential) presents high value of peak power such as 2500 kW, because of their heating space to satisfy. On the other hand, residential buildings are aligned with normal values of 20-25 kWp.

Loads, Mass Flow Rate, Supply and Ground Temperature

Once obtained the right power demand for the 271 buildings analysed, the next step to fill in the input of HeatLoads and MassFlowRate excel spreadsheets in *NeMo* is to associate to the substations of the DHN every 271 structures according to some criteria, such as closeness, same end-uses buildings provides, and zone of the city.

In this way, it is easy to achieve the thermal power of the nodes by the sum of the buildings' power demand associated to the single consumer node.

An example of association between substations and edifices is reported in the next figure:

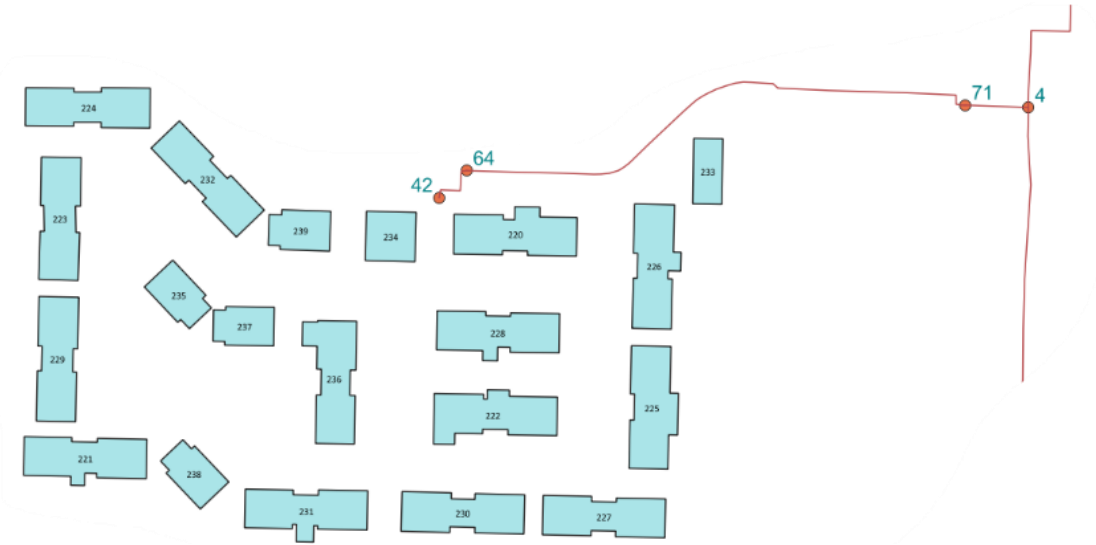


Figure 4.11: Example of association between buildings and node 42.

In the previous picture is shown the clear association between the residential complex of the structures and the node 42. The results of grouping are divided among West and East DHN.

Substations	Associated ID Buildings
1	19, 80, 81, 84, 298, 301, 303, 322, 336, 337
15	267, 268, 271
18	290, 291, 292, 293, 295, 296, 297, 321
27	275, 278, 287
38	17, 78, 323, 324
42	from 220 to 239
43	107, 108
44	15, 16
48	269, 270, 272
73	89, 90, 91, 92, 93, 94, 95, 96, 97, 98, 99, 100, 101, 102, 326, 327, 328
76	195
77	253, 256, 258, 260
81	14
89	282, 284, 286, 289
94	255, 257
98	241, 249, 252
101	277, 279, 280, 288
105	240, 245, 247, 294
113	254, 259

120	302, 311
124	242, 243, 244, 246, 248, 250, 251
125	209, 210
126	104, 105
129	20, 83, 213, 215, 217, 219, 310
132	211, 306
136	85, 88, 318, 319, 320
138	276, 281, 283, 285
142	212, 214, 216, 218, 307, 309
145	13, 86, 87
156	261, 262, 263, 264, 265, 266, 273, 274

Table 4.9: Association between buildings and nodes of the DHN West part.

Substations	Associated ID Buildings
10	21, 22, 23, 131, 132, 139, 140, 143, 145, 149, 150
12	33, 42, 49, 61, 69
13	6, 317
14	35, 41, 47, 60, 70
19	2, 54
28	110, 115, 116, 118, 120, 121, 124, 127, 316
30	66
33	111, 112, 113, 114, 117, 119, 122, 123, 125, 126, 128
34	30, 32, 38, 45, 46, 51, 59, 68
55	18, 106
58	5
75	25
80	1
82	26
84	300
87	29, 312, 313, 314, 315, 332
90	24
91	31, 34, 36, 40, 43, 44, 48, 50, 52, 53, 55, 56, 57, 62, 63, 64, 65, 67, 71, 72, 73, 75, 334
104	3
107	37
111	4, 27
112	28, 308
114	299
123	39, 58, 74, 330, 333
144	129, 130, 133, 134, 135, 136, 137, 138, 141, 142, 144, 146, 147, 148, 151, 152, 197, 200, 205
147	103, 304, 305, 335

Table 4.10: Association between buildings and nodes of the DHN East part.

As it can be noticed, in the West part of the DHN there are 145 edifices associated to 30 substations, instead, in the East one there are 126 buildings and 26 associated consumer nodes.

At this point, the spreadsheet HeatLoads inside the Loads input file in *NeMo* has been completed, because the hourly thermal power of substations has been found out with the mentioned method.

Once the HeatLoads spreadsheet inside the Loads input file has been completed with the mentioned method, the succeeding step was focused on the calculation of the linked mass flow rate to the thermal power of the substations, but before this, the supply temperature of the supply station must be determined by means of the climatic curve shown in Fig. 4.13.

To simulate a realistic behaviour of a DHN, it has been decided to modify the supply temperature over the days according to a climatic curve, in the way to provide 60°C when the outdoor temperature is higher than 15°C and, on the other hand, 90°C when it is less than -10°C. When $T_{outdoor}$ reaches values between -10°C and 15°C, T_{supply} is obtained by means of an interpolation formula presented subsequently:

$$T_{supply} = T_{supply,max} - (T_{supply,max} - T_{supply,min}) \frac{T_{outdoor} - T_{outdoor,min}}{T_{outdoor,max} - T_{outdoor,min}} \quad (4.15)$$

Where:

- $T_{supply,max} = 90^{\circ}C$,
- $T_{supply,min} = 60^{\circ}C$,
- $T_{outdoor,min} = -10^{\circ}C$,
- $T_{outdoor,max} = 15^{\circ}C$.

The hourly outdoor temperature of Aalborg has been taken from the Danish Meteorological Institute – DMI API (<https://dmigw.govcloud.dk/v2/climateData/api>), with the possibility to opt for different years of surveys, in particular, for this case study, it has been selected year 2021. The resulting outdoor temperature plot is shown in Fig. 4.12:

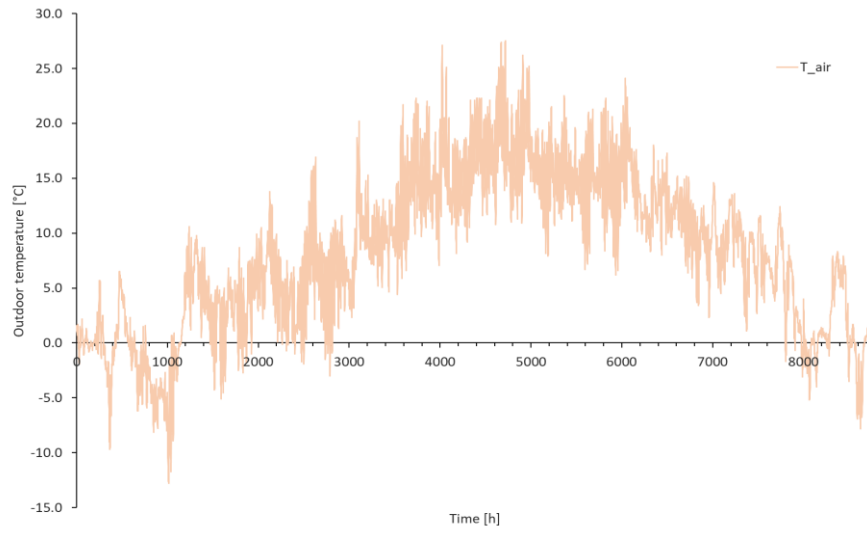


Figure 4.12: Outdoor temperature profile.

The climatic curve for the supply temperature profile is specular:

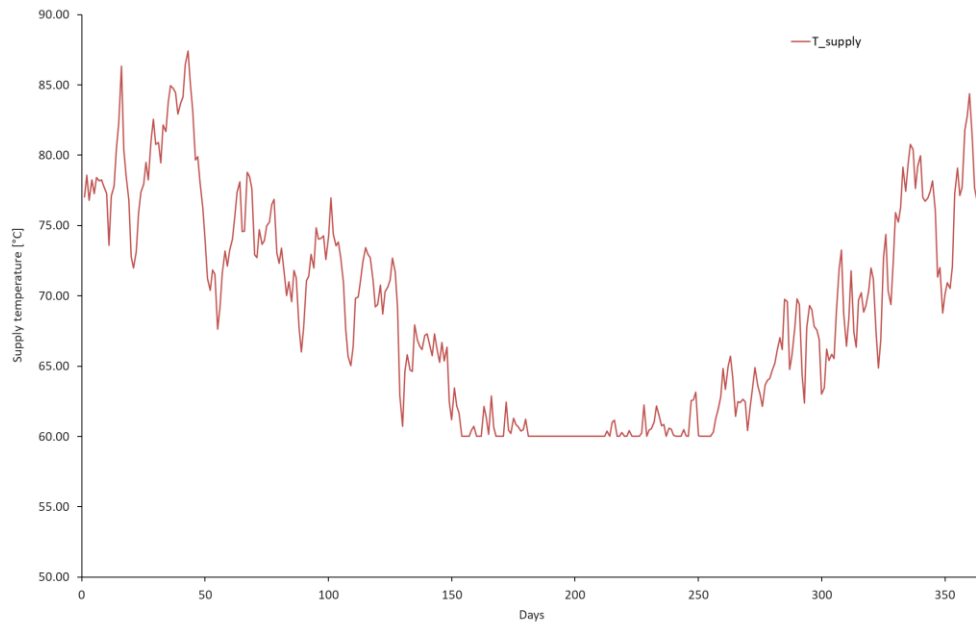


Figure 4.13: Climatic curve for the supply temperature of the supply station.

The latter step to fill in the Loads input file of *NeMo* is the estimation of the hourly mass flow rate to the substations. This term is obtained by the known formula of an heat-exchanger:

$$\dot{m} = \frac{q}{c_p \Delta T} [kg/s]$$

(4 . 16)

Where:

- q is the hourly substation thermal load [kW],
- c_p is the specific heat of the fluid, i.e. $c_{p,water}=4.187$ kJ/(kg K),
- ΔT is the difference between the supply temperature, time-dependent, and a fix return temperature.

Regarding the parameter ΔT , it is assumed to be constant for all the nodes at a certain day, but due to the variability of the supply temperature, which is regulated by the climatic curve, the value of ΔT change among the examined days.

This assumption of constant ΔT between the nodes is the result of a statistic process, realized analysing some values of T_{supply} and T_{return} of the considered substation (indicated in table 4.9, 4.10) sent by Aalborg Forsyning with the shapefile of the network, as expressed in Chapter 3.

This statistic process mentioned above consists in the average of supply temperature, return temperature, and ΔT of the users presented in the Attribute Table of the related QGIS layer, and the calculation of the associated standard deviation.

The results are reported in the next table:

	Average Temperature [K]	Standard Deviation [K]
Supply temperature	359.06	1.53
Return temperature	317.99	2.39
ΔT	41.07	1.51

Table 4.11: Statistic results for the constant ΔT assumption.

With this low values (<5%) of standard deviation, the constant assumption on the ΔT is considered realistic and reliable.

Note: *NeMo* functioning has a weakness on the mass flow rate, indeed it doesn't accept a zero value on this, as the simulation doesn't work. Therefore it has been opted for keeping a certain value of mass flow rate (5% of the max in the whole

simulation-time) instead insert zero values when the heat load isn't required. The results of this assumption are explained in chapter 6.

As regard the second file *Subs*, it is required to declair which ID substations are suppliers and which are consumers. All the substations obtained from the buildings ID association shown in table 4.9, 4.10 are consumers, the only supplier is the node 8, derived from the cement factory.

The third file *Net* is compiled by the Attribute Table attached in the pipe layer of QGIS shapefile.

The next file is related to the undisturbed ground temperature. The most important factors affecting heat transfer are the difference between ambient and fluid temperatures and the thermal insulation. For direct-buried piping, the ambient temperature is the soil temperature. For buried systems, the undisturbed soil temperatures may be estimated for any time of the year as a function of depth, soil thermal properties, and prevailing climate.

The following equation has been used to estimate the undisturbed ground temperature at any depth at any point during yearly weather cycle (ASCE 1996):

$$t_{s,z} = t_{ms} - A_s e^{-z\sqrt{\frac{\pi}{\alpha\tau}}} \sin\left[\frac{2\pi(\theta - \theta_{lag})}{\tau} - z\sqrt{\frac{\pi}{\alpha\tau}}\right] \quad (4.17)$$

Where:

- t_{ms} is the mean annual surface temperature, 8.12 °C,
- A_s is the surface temperature amplitude, 8.66 °C,
- z is the depth, 1 m,
- α is the thermal diffusivity of the ground, m²/h,
- τ is the annual period, 8760 hours,
- θ is the related hour,
- θ_{lag} is the phase lag of soil surface temperature, 2819.93 hours

The thermal diffusivity is a made up of several terms, and the connected formula is:

$$\alpha = \frac{24 \times 3600 k_s}{1000 \rho_s [c_s + c_w(w/100)]} = \frac{86.4 k_s}{\rho_s [c_s + 4.18(w/100)]} = 0.0018391 \left[\frac{m^2}{h} \right] \quad (4.18)$$

Where:

- ρ_s is the soil density, 2500 kg/m³,
- c_s is the dry soil specific heat, 0.73 kJ/(kg K),
- c_w is the specific heat of water, 4.187 kJ/(kg K),
- w is the moisture content of soil, 20 % (dry basis)
- k_s is the soil thermal conductivity, 2 W/(m K)

c_s is considered 0.73 kJ/ (kg K) because is nearly constant for all type of soil, the moisture is considered usually as 20%.

With this parameters, the resulting undisturbed temperature of the ground profile compared to outdoor, surface and average temperature is:

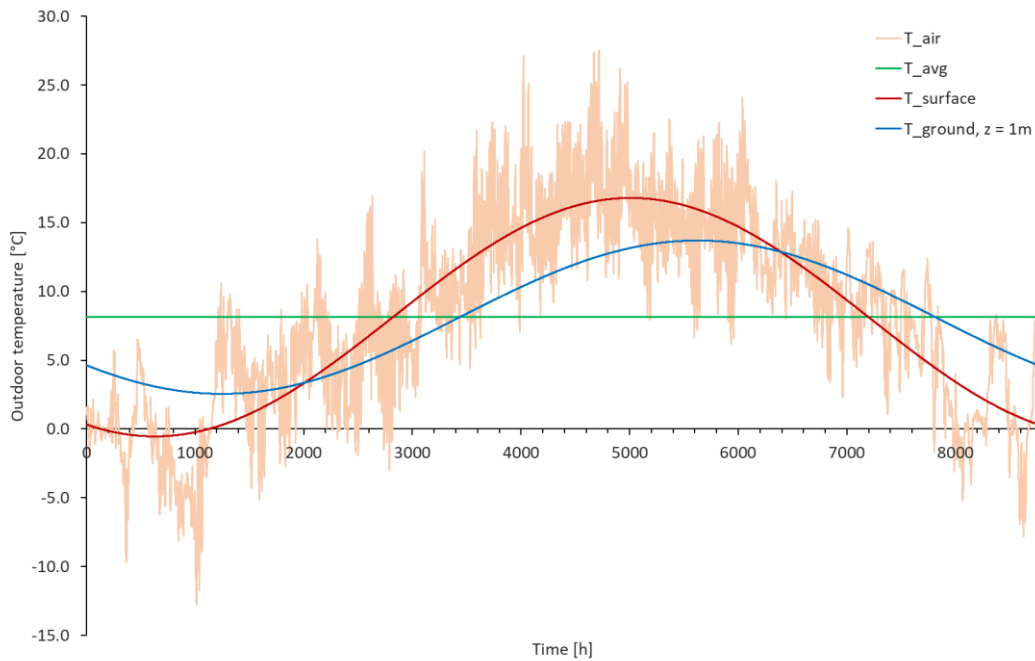


Figure 4.14: Ground temperature profile compared to the surface, average, and outdoor one.

The ground temperature is clearly shifted on the right compared to the surface one, because of the sine argument, thanks to the depth factor z preceded by the minus. Moreover, the width of the wave is reduced due to the presence of the same depth value in the A_s term. Increasing the depth leads to constant values of ground temperature with a more shifted peak in order to overlap, at higher depth, the average temperature profile reported as green line.

Parameters

The simulation has now all the input that it needs to run, except for the parameters explained in table 4.12:

Parameters	Unit	Value
Timestep of input	min	60
Simulation time	hours	2520 ¹
Tolerance T1	kg/s	0.001
Tolerance T2	Pa	50
Threshold mass flow rate	kg/s	0.007
Solver	LS	
Max length of pipe elements	m	500
Solver time step	s	300

Table 4.12: Parameters of the simulation.

¹The simulation time-step is 2520 hours, because it has been assumed a heating period similar to the Italian one, i.e., 15th October – 15th April, but as the simulation starts in the 1st day of 2021, the examined period has become 1 January 2021 – 15 April 2021. Moreover, *NeMo* doesn't work during period of contemporary absence of loads for all the substations, as in the summer, because it needs a substation load reference different from zero value.

Chapter 5

Clustering

The last step of this work regards the clustering of the original network in order to obtain different equivalent networks with a smaller number of nodes and pipes, to reduce the computational effort of the simulation tools, i.e., the elapsed time of the simulation, keeping the same features such as the total mass flow rate, the total heat losses, the total water volume, or the total thermal power unchanged. The clustering functions implemented in MATLAB follow a tree-network type method called Danish Method.

5.1 Collapsing a network tree into one branch – step 1

A DH network with a pure tree structure has no circular connections and only one production plant. The method presented in this chapter gradually reduces an original tree network to an equivalent single branch network so that all pipes are connected sequentially, and heat consumers are connected to pipe junctions along the branch. By using this method of reduction, the total number of pipe branches and nodes (junctions) is not reduced, but the total length of pipes is reduced. Thus, the resulting branch typically consists of very short pipes.

In Fig. 1, the left side shows that a DH network with no circular loops consists of several two-branch subnetworks, where the branches (1 and 2) originating from the same node 0 lead to the nodes 1 and 2. Each branch represents a pair of supply and return DH pipes.



Figure 5.1: Collapse of the branch 1 in the branch 2 – step 1.

Let the delay time be the time it takes the water to go through a pipe branch. It is assumed that the delay time in branch 1 is less than the delay time in branch 2. Typically, the simple network in Fig. 5.1, is part of a more complex network, and therefore, other DH network trees might, in principle, be connected to nodes 1 and 2.

In the sequel, the sub-network mentioned above is transformed into a simpler equivalent network, as shown in the right side of Fig. 5.1. By eliminating branching, and reducing the total length of the branches, the equivalent network is simpler compared to the original. From now on, the branch from node 0 to node A will be named branch A, and the branch between nodes A and B will be named branch B. Assuming that supply temperature and flow are the same at node 0 in the two networks, the equivalent network meets the following conditions:

- The return temperature in node 0 is the same for the two networks,
- The sum of the loads in nodes A and B is equal to the sum of the loads in nodes 1 and 2,
- The total heat loss from branches A and B is equal to that from branches 1 and 2,
- The total water volume in branches A and B is equal to that in branches 1 and 2.

The steel in the DH pipes is included in the model by interpreting velocity v and delay τ as connected to the propagation of a temperature front and by assuming that the temperatures of the pipe wall and the water are the same in every cross-section of the pipe. Ignoring the steel pipe is equivalent to assigning the value one to the variables $\varphi = C^w / (C^w + C^p)$ and $\psi = \varphi_2 / \varphi_1$.

The following is assumed:

- The time delay in branch 1 is less than or equal to the time delay in branch 2, or $\tau_1 \leq \tau_2$,
- The mass flows in branches 1 and 2 are varying proportionally with time, i.e., $\alpha = m_2 / m_1$ is constant through time.
- The time delay in branch A is equal to the delay in branch 1:

$$\tau_A = \tau_1 \tag{5.1}$$

- The time delay in branches A and B is equal to the delay in branch 2:

$$\tau_B = \tau_2 - \tau_1 \quad (5.2)$$

- The water volume is conserved:

$$V_A + V_B = V_1 + V_2 \quad (5.3)$$

- The mass flow is conserved (notice that m denotes mass flow in a heat-exchanger, not a DH pipe)

$$m_A + m_B = m_1 + m_2 \quad (5.4)$$

- The heat load is conserved:

$$P_A + P_B = P_1 + P_2 \quad (5.5)$$

- The heat loss from the pipes is conserved:

$$Q_A + Q_B = Q_1 + Q_2 \quad (5.6)$$

To obtain the equivalent network, it has been chosen:

- Branch B equal to the last part of branch 2, i.e., the part of branch 2 with $\tau > \tau_1$. This choice doesn't take the insulation of pipe B into account:

$$d_B = d_2 \quad (5.7)$$

$$D_B = D_2 \quad (5.8)$$

$$A_B = A_2 \quad (5.9)$$

$$\varphi_B = \varphi_2 \quad (5.10)$$

- The mass flow in branch B is equal to that in branch 2:

$$m_B = m_2 \quad (5.11)$$

- The velocity in branch A equals a weighted average of the velocities in branches 1 and 2. To give priority to the branch with the bigger flow, the

mass flows are used as weight factors:

$$v_A = \frac{m_1 v_1 + m_2 v_2}{m_1 + m_2} \quad (5.12)$$

We now derive the remaining characteristics of the equivalent network, which follow from the above definitions:

$$m_A = m_1 \quad (5.13)$$

$$V_A = V_1(1 + \alpha)(\varphi_A/\varphi_1) \quad (5.14)$$

$$V_B = V_2(1 - \gamma\psi)$$

$$L_B = L_2(1 - \gamma\psi) \quad (5.15)$$

$$L_A = L_1 \frac{(1 + \alpha^2\psi A_1/A_2)}{\beta} \quad (5.16)$$

$$d_A = 2 \sqrt{\frac{\beta(1 + \alpha\psi)A_1A_2}{(A_2 + A_1\alpha^2\psi)\pi}} \quad (5.17)$$

$$D_A = d_A \sqrt{1 + \left(\frac{\rho^w c^w}{\rho^p c^p}\right) \left(\frac{1 - \varphi_A}{\varphi_A}\right)} \quad (5.18)$$

To this point, the insulation of the pipe has been excluded from the calculation. When calculating the heat loss from a pipe, it is used the temperature at the inlet to the pipe. Since the heat loss in a pipe and the temperature drop along the pipe are small, the error introduced by using the inlet temperature is acceptable. The total heat loss in the two systems should be equal, which imposed that the total balance is defined as:

$$\begin{aligned} (T^s - T_G)(H_A^s + H_B^s) + (T_{AB} - T_G)H_A^r + (T_B^r - T_G)H_B^r \\ = (T^s - T_G)(H_1^s + H_2^s) + (T_1^r - T_G)H_1^r + (T_2^r - T_G)H_2^r \end{aligned} \quad (5.19)$$

While T_A^r is the return temperature from the load in node A before mixing with the water from branch B, T_{AB} is the temperature in node A after mixing has taken

place. By demanding that both networks have the same return temperature in node 0:

$$T_{AB} = \frac{T_1^r + \alpha T_2^r}{\beta} \quad (5.20)$$

We choose to let the two networks have the same amount of heat loss on the supply side, which results in the following equation for the heat conductivity out of the supply pipes:

$$H_A^s + H_B^s = H_1^s + H_2^s \quad (5.21)$$

Now we demand that the total heat load in the equivalent network should equal the total load in the original network, and we obtain the following terms:

$$T_A^r = T_1^r \frac{\frac{\theta_A^r \alpha}{\beta} + \theta_B^r - \alpha}{\theta_B^r} + T_2^r \frac{\left(\frac{\theta_A^r \alpha}{\beta} + \theta_B^r - \theta_2^r\right) \alpha}{\theta_B^r} + T_G \frac{(1 + \theta_2^r - \theta_A^r - \theta_B^r) \alpha}{\theta_B^r} \quad (5.22)$$

$$T_B^r = T_1^r \frac{1 - \frac{\theta_A^r}{\beta}}{\theta_B^r} + T_2^r \frac{\theta_2^r - \frac{\theta_A^r \alpha}{\beta}}{\theta_B^r} + T_G \frac{\theta_A^r + \theta_B^r - \theta_2^r - 1}{\theta_B^r} \quad (5.23)$$

$$P_B = P_1 \frac{\alpha \left(1 - \frac{\theta_A^r}{\beta}\right)}{\theta_B^r} + P_2 \frac{\theta_2^r - \frac{\theta_A^r \alpha}{\beta}}{\theta_B^r} + P_G \frac{\theta_A^r + \theta_B^r - \theta_2^r - 1}{\theta_B^r} \quad (5.24)$$

$$P_A = P_1 \frac{\frac{\theta_A^r \alpha}{\beta} + \theta_B^r - \alpha}{\theta_B^r} + P_2 \frac{\frac{\theta_A^r \alpha}{\beta} + \theta_B^r - \theta_2^r}{\theta_B^r} - P_G \frac{\theta_A^r + \theta_B^r - \theta_2^r - 1}{\theta_B^r} \quad (5.25)$$

$$H_B^r = H_2^r (1 - \gamma \psi) \quad (5.26)$$

$$H_A^r = \frac{(\Delta T_1 H_1^r + \Delta T_2 H_2^r \gamma \psi) \beta}{\Delta T_1 + \alpha \Delta T_2} \quad (5.27)$$

$$H_B^s = H_2^s (1 - \gamma \psi) \quad (5.28)$$

$$H_A^s = H_1^s + \gamma\psi H_2^s \quad (5.29)$$

Where:

- $\alpha = m_2/m_1$,
- $\beta = 1 + \alpha$,
- $\theta_x^r = H_x^r/H_1^r$,
- $P_G = m_2 c_{p,w}(T^s - T_G)$ is the heat load that would be delivered in node 2 if the DH water were cooled to ground temperature T_G instead of T_2^r ,
- $\gamma = (V_1/V_2)(m_2/m_1)$.

The conservation of heat loss can be expressed now as:

$$(T_{AB} - T_G)H_A^r + (T_B^r - T_G)H_B^r = (T_1^r - T_G)H_1^r + (T_2^r - T_G)H_2^r \quad (5.30)$$

5.2 Removing internal nodes – step 2

In the equivalent network, which is formed by converting a DH network consisting of many branches into an equivalent network, the nodes will be positioned close to each other, separated by relatively short pipes. Following the method described in the sequel, such nearby nodes can be collapsed to simplify the equivalent network further. By using this method, it is also possible to reduce the equivalent network to just a few or just a single branch. Consequently, the quality of the resulting network model will be reduced.

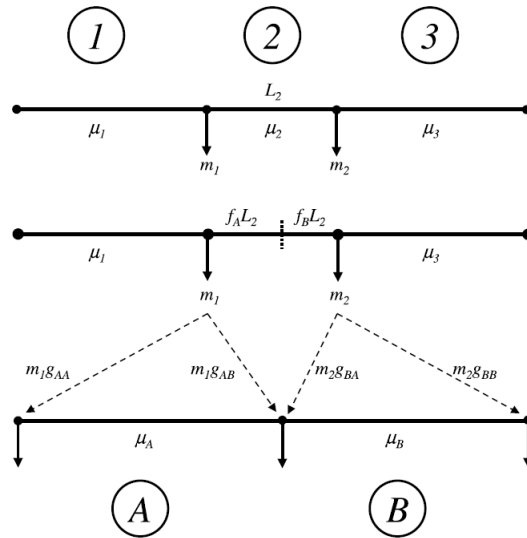


Figure 5.2: Removing internal nodes – step 2.

Let indices 1, 2 and 3 describe the three branches in the original DH network, while indices A and B describe the slightly changed replacements for branches 1 and 3 as shown in Fig. 5.2. We will divide branch 2 into two parts and let branch A represent branch 1 and the first part of branch 2, while branch B shall represent the other part of branch 2 and branch 3. In this section, we will use μ to indicate flow in the branches, while m , as in the previous sections, indicates flow to heat exchangers. Based on this, the following identities can be drawn:

$$m_1 = \mu_1 - \mu_2 \quad (5.31)$$

$$m_2 = \mu_2 - \mu_3 \quad (5.32)$$

Branch 2 is not divided into equal parts, but it is divided so that the length of the first part is $f_A L_2$, and the second one is $f_B L_2$, where:

$$f_A = \frac{m_2}{m_1 + m_2} \quad (5.33)$$

$$f_B = \frac{m_1}{m_1 + m_2} = 1 - f_A \quad (5.34)$$

By defining factors f_A and f_B in this way, the larger part of branch 2 is included in branch B if load 1 is much bigger than load 2, and therefore, in this case, branch A will be almost identical to branch 1.

The load (or more correctly flow to the heat exchanger) in node 1 is split into two parts. Symbols g_{AA} and g_{AB} indicate the fractions of the load that are moved to the first and to the last end, respectively, of branch A. Likewise, g_{BA} and g_{BB} indicate the fractions of the load in node 2 that are moved to the first and to the last end of branch B. Fig. 5.2 shows how the g-factors are used.

The g-factors are defined using time delay [s] as follows:

$$g_{AA} = \frac{f_A \tau_2}{\tau_1 + f_A \tau_2} \quad (5.35)$$

$$g_{AB} = \frac{\tau_1}{\tau_1 + f_A \tau_2} \quad (5.36)$$

$$g_{BA} = \frac{f_B \tau_2}{\tau_3 + f_B \tau_2} \quad (5.37)$$

$$g_{BB} = \frac{\tau_3}{\tau_3 + f_B \tau_2} \quad (5.38)$$

By defining the g-factors in this way, the major part of the load is moved to the closest node in the simplified network. It is readily seen that:

$$g_{AA} + g_{AB} = g_{BB} + g_{BA} = 1 \quad (5.39)$$

The flow in branches A and B: can be expressed by:

$$\mu_A = \mu_1 - g_{AA} m_1 \quad (5.40)$$

$$\mu_B = \mu_2 - g_{BA} m_2 \quad (5.41)$$

To find branch A from the data describing branches 1 and 2, and branch B from the data describing branches 2 and 3, it is necessary that the total length, time delay, water volume and heat losses should be preserved. The preservation of length can be expressed by:

$$L_A = L_1 + f_A L_2 \quad (5.42)$$

$$\tau_A = \tau_1 + f_A \tau_2 \quad (5.43)$$

$$V_A = V_1 \frac{\mu_A \varphi_A}{\mu_1 \varphi_1} + f_A V_2 \frac{\mu_A \varphi_A}{\mu_2 \varphi_2} \quad (5.44)$$

$$X = \frac{\rho^p c^p}{\rho^w c^w} \quad (5.45)$$

$$V_A^p = V_A \frac{1 - \varphi_A}{\varphi_A X} \quad (5.46)$$

$$d_A = 2 \sqrt{\frac{V_A}{\pi L_A}} \quad (5.47)$$

$$D_A = 2 \sqrt{\frac{V_A + V_A^p}{\pi L_A}} \quad (5.48)$$

$$h_A = \frac{h_1 L_1 + f_A h_2 L_2}{L_A} \quad (5.49)$$

In a similar way, these data can also be found for branch B.

For the complete equations of the Danish Method implemented in this work, the paper reference is mentioned in ‘Aggregated dynamic simulation model of district heating network’.²³

The Danish Method has been applied starting from the ‘leaf of the network tree’, or rather, the extreme consumer nodes for the step 1, as indicates in the figure 5.3. Afterwards, the step 2 has been utilized whenever, after step 1, four nodes, or equally, three pipes, were aligned to remove the internal nodes, as shown in the next Fig. 5.4.

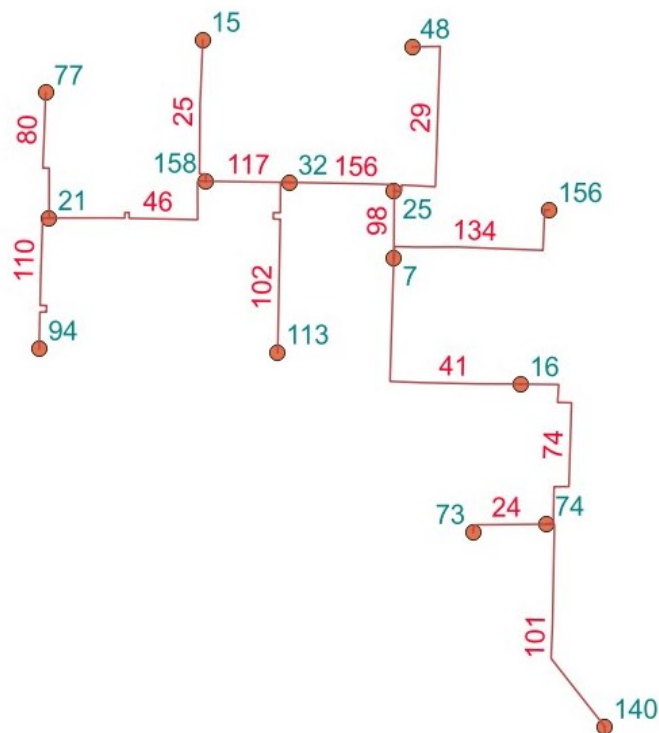


Figure 5.3: Starting configuration of the North-West part of DHN.

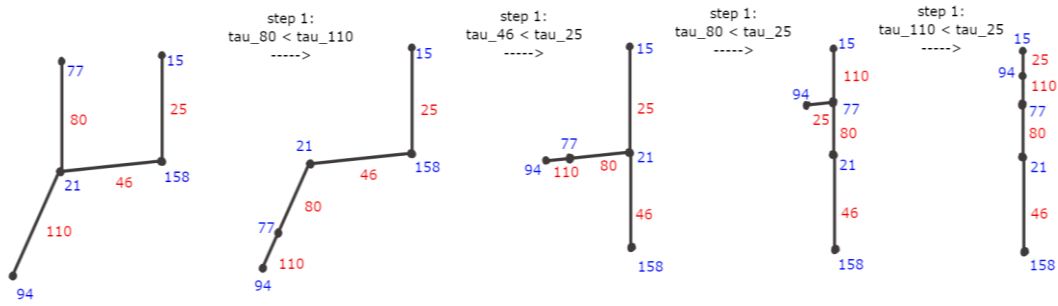


Figure 5.4: Following step 1 (collapsing node) to align the nodes and pipes for step 2 (removing internal nodes).

In Fig. 5.4 are presented the needed step 1 to modify the network from the original structure, according to τ of every pipes compared, for the utilization of the step 2. The functions has been created in MATLAB allow to correctly reproduce step 1 and 2, in order to modify the *NeMo* input Power and Mass Flow Rate Matrix for 2520 hours, i.e., the time of the simulation, according to the method.

However, these functions doesn't modify the Incidence Matrix automatically, and consequently, the Edge List of the analysed network. Following the variation of the network topology between every steps, it has been possible to manually draw up the new Edge List.

These automatization process of the functions can be refine as next step of this work.

Chapter 6

Results

In this chapter the results of the simulation done by *NeMo* are presented, as for the base case study with 157 branches and 158 nodes, and the equivalent networks obtained by the clustering functions.

6.1 Original case study

The features presented in this paragraph deals with the thermal heat losses between the supply station and one of the farthest node, chosen for the ID node 48, because it will be the last node of the north-west equivalent network after the clustering, in order to compare the results between equivalent and original network for the same node.

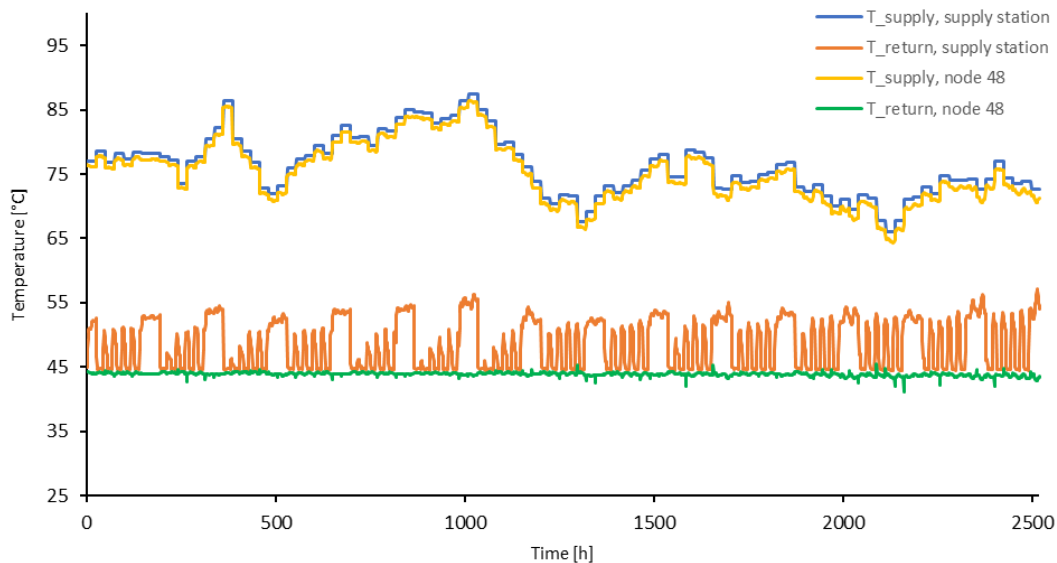


Figure 6.1: Different profiles of supply and return temperature among supply station and node 48.

As shown in Fig. 6.1 the heat losses between the supply station and the critical node are visible by means of the different supply temperature profile. As regards the return temperature, the effects on the critical nodes should be the same: the return temperature on the supply station must decrease compared to the critical one, as the water volume return to the supplier, due to the propagation of heat losses through the pipes, but this is not happened. The reason of the different effect between supply and return temperature deals with the absence of heat load

in the weekend as consequence of the plant availability for office and service buildings. The return temperature of the critical node is linear due to the heat provide to residential buildings, where plant availability is always on, as reported in Chapter 4.

In this way, the return temperature in the supply station is affected by those substation without a heat exchange, despite a mass flow travelling in the pipe due to *NeMo* functioning (5% of the max mass flow, as explained in the note, page 50). The return temperature in this substation is consequently equal to the supply temperature, and the return pipes presents a higher T_{ret} because of the mixing of this amount of non-exchange water.

This is the reason of the return temperature peaks on the supply station, that leads to different effect compared to the one on the supply temperature.

The thermal balance implemented in *NeMo* for all the nodes considers the thermal inertia of the fluid as a term, and this leads to give, in the first hours of the days, when the supply temperature change, a higher value of the supply temperature between consumers and supplier due to the dynamic behaviour of the network, as the consumers need time to adapt.

This influence is shown in the next Fig. 6.2:

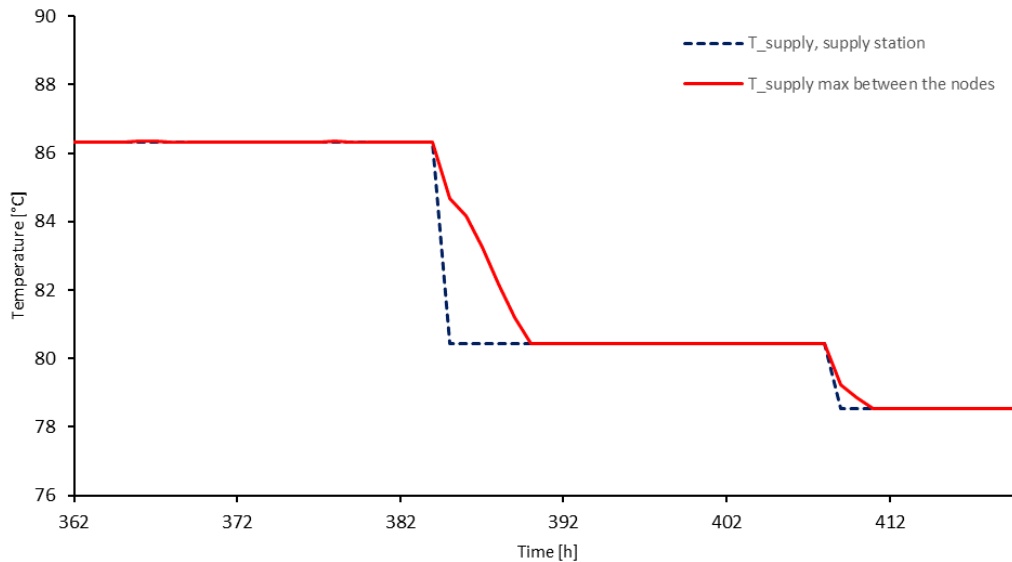


Figure 6.2: Representation of thermal inertia of the fluid in the changing of supply temperature by supply station

As revealed, the consumers need time to adapt to the dynamic behaviour of the network, so in the first hour after the change, the supply temperature of the supply

station is consequently lower. This effect is presented for this period (hour 362-hour 420) because of its visible difference. As it can be seen, the situation is restored after few hours.

The focus on the heat losses due to the path between supplier and critical consumer chosen is presented, for a certain hour (hour 24), in the Fig. 6.3:

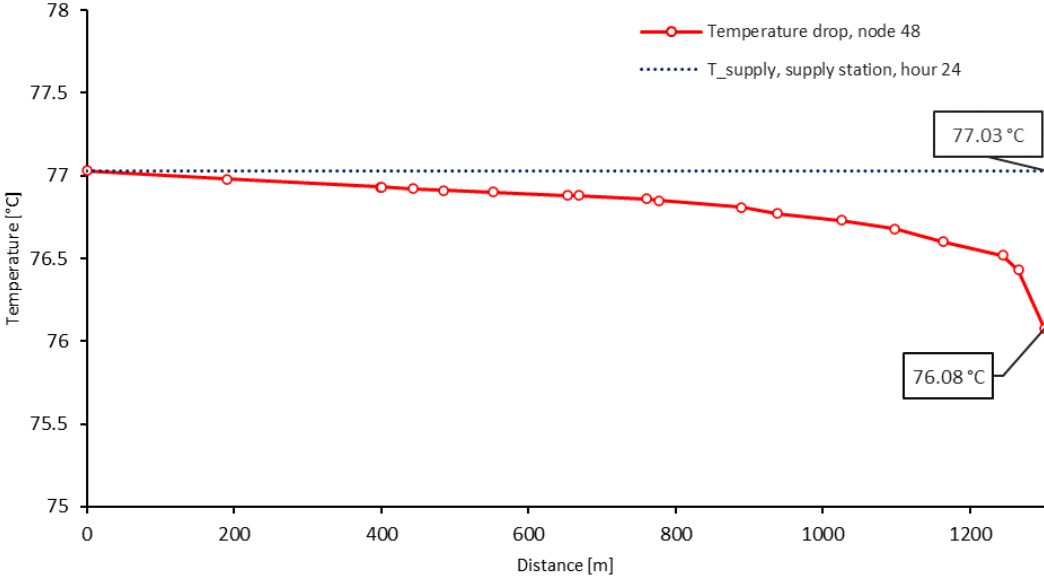


Figure 6.3: Node 48 temperature drop related to the distance from supply station, at hour 24.

The temperature drop on the ID node 48 is presented above: following the path to reach the related node, the heat losses along the pipe due to the ground temperature, decrease the fluid temperature, as the distance improve, in order to give at the consumer 48 the outlet fluid temperature of 76.08°C. The temperature drop between supplier and consumer is about 1°C for 1301.36 m of distance, thanks to the optimal insulation arranged by the layers of PU and steel that cover the ducts.

As regards the whole network heat losses, the following plots explains in a detailed way the linked trend during the weeks:

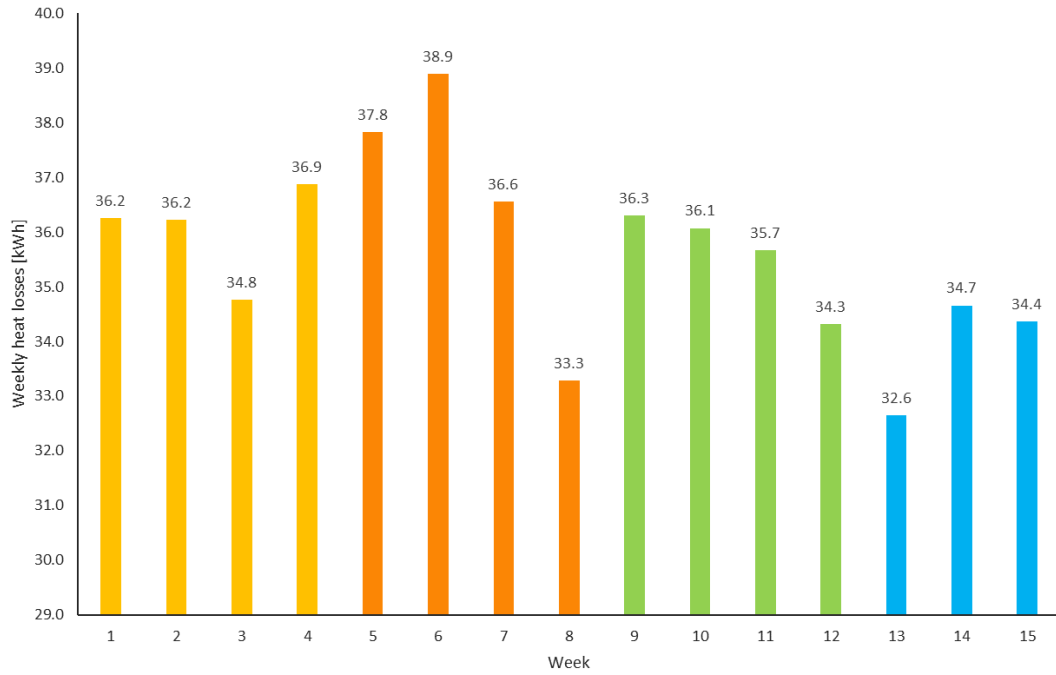


Figure 6.4: Weekly heat losses of the whole network.

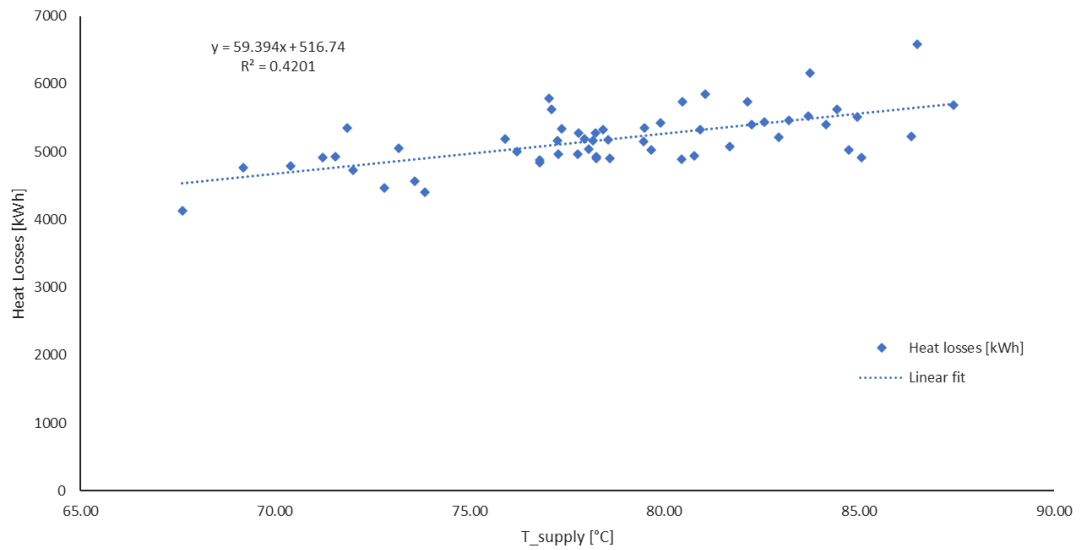


Figure 6.5: Linear trend of the network heat losses related to the supply temperature of the supply station.

In the Fig. 6.4 the period of simulation, i.e., 1 Jan 2021 – 15 Apr 2021, has been divided into 15 weeks, and the related amount of thermal losses [kWh] has been calculated. The results deals with the outdoor temperature (and to the supply temperature, that is linked to the air temperature by the climatic curve explained

in the Chapter 4): the decreasing of the external temperature bring the supply one to higher values, and the heat losses increase. Indeed, it is clear the reduced amount of heat losses as the days are getting closer to the spring season, expressed by the azure column.

As a confirmation of this, the second pictures demonstrates the proportional influence of the supply temperature. This type of plot is usually referred to the average temperature of the fluid instead of the supply one. In this case, this latter parameter isn't representative of the avg temperature because it is influenced by the return one too, which is non-linear due to the existence of peak explained as a results of the mass flow presence's when the heat load isn't requested by consumers. The proportional trend is, anyway, clear, also compared to the supply temperature.

6.2 Clustered case study

The equivalent network, obtained by the functions implemented in MATLAB related to the step 1 and step 2 of the Danish Method, has reduced the number of nodes and branches more than 15%, in particular, the new cluster network has 22 nodes and 22 branches less, compared to the original one.

The following nodes and pipes has been removed:

Nodes	Branches
1	13
15	25
21	39
24	46
25	61
27	71
32	72
35	76
43	80
61	87
77	98
78	100
88	102
89	106
92	110
94	116
101	117
113	134

138	149
148	154
156	155
158	156

Table 6.1: ID of nodes and pipes removed from the original network.

The thermal peak power, the total water volume and the total heat losses coefficient are equal to the original network, but the length, according to the cluster Danish method, hasn't been conserved, as reported in the table 6.2:

	Original Network	Equivalent network
Thermal Peak Power [MW]	34.945	34.945
Water Volume [m ³]	167.82	167.82
Total Heat Losses Coeff. [W/K]	1779.35	1779.35
Length [km]	7.88	7.32

Table 6.2: Conserved properties between original and equivalent network.

All the pipes and nodes labels have been re-assigned, in order to adjust the new incidence matrix, otherwise, with the old labelling, during the calculation of the incidence matrix there would be some empty lines and columns, corresponding to the ones removed, that didn't allow to pursue with the simulation.

Moreover, beyond the necessity of new labelling, NeMo needs as characteristics of the pipe the diameter and the thermal conductivity of the insulation. As the new inner and outer diameter of the ducts has values which can't be found in the standard pipes catalogue, it has been assumed a standard thermal conductivity, typical of PU insulation, of 0.0029 W/(m K), and then the corresponding diameter of the insulation has been calculated as:

$$d_{ins} = d_{out} e^{\frac{2\pi k}{h_s}}$$

Where:

- d_{out} is the outer diameter of the pipe,
- k is the thermal conductivity of the insulation,
- $h_s = H/L$ is the heat losses coefficient [W/m K].

The results of the simulation has been presented subsequently:

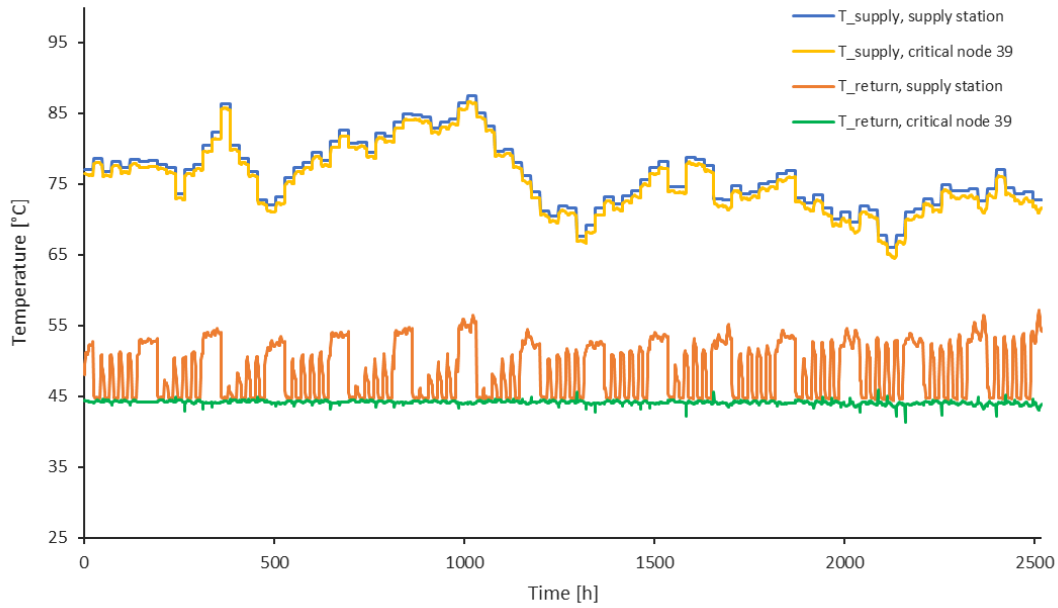


Figure 6.6: Supply and return profiles temperature of node 39 (ex 48) and supply station for the equivalent network.

The first plot indicates the heat losses of the node 39 (ex 48) and demonstrates the reliability of the simulation compared to the original network. The new supply temperature profile, expressed in yellow line, doesn't have visible differences with the old one, and the behaviour of the return temperature is more than similar. Some slight differences are presented in the next figure, as the conservation of the features between original and equivalent network is thought for the nominal conditions, instead, out of design conditions the features can slightly change.

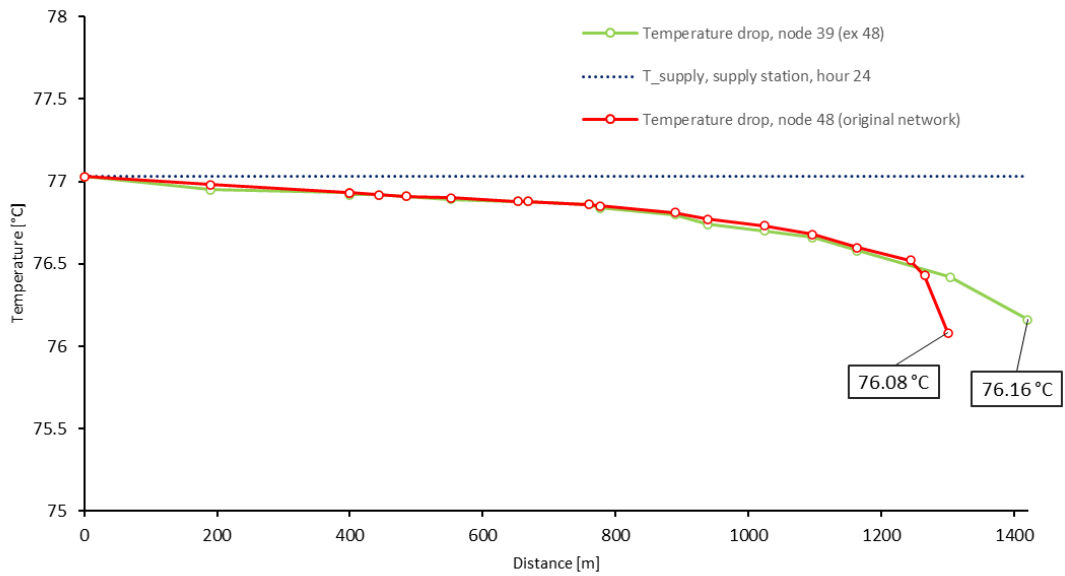


Figure 6.7: Comparison between temperature drop of old node 48 and new node 39 (ex 48) related to the distance.

The temperature drop between node 39 and original 48 is substantially overlapped, until the clustering took place. Afterwards, the clustering network is farther from the supply station at the node 39 because of non-conservation of the length in the Danish Method, this is the reason of the difference of distance. The value of temperature drop is marginally different for 0.08°C , as announced previously.

Another important characteristics conserved by the clustered network is the thermal inertia of the fluid, evaluated in the same period of the one in the analysis of the original network, i.e. hour 362 – hour 420, as shown in Fig. 6.8.

In this figure, it can be noticed, again, the trivial differences between the two networks in out-of-design conditions, more accentuated in the second drop compared to the first one. In general, the two output profiles corresponds.

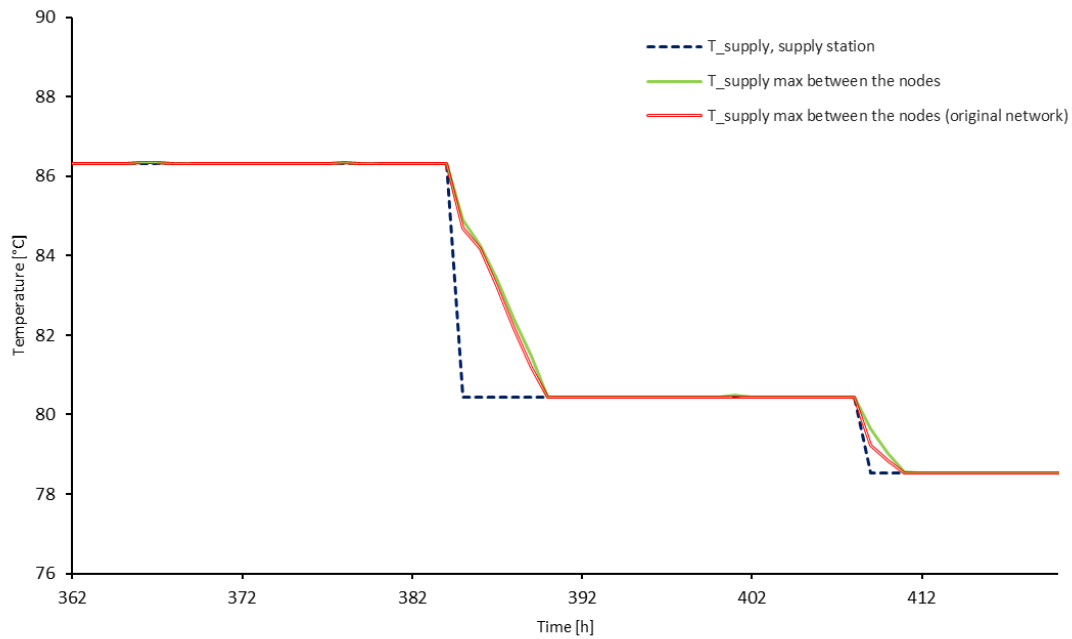


Figure 6.8: Comparison of thermal inertia term between the original and equivalent networks.

As regards the whole network heat losses, the comparison has been done with the next column plot:

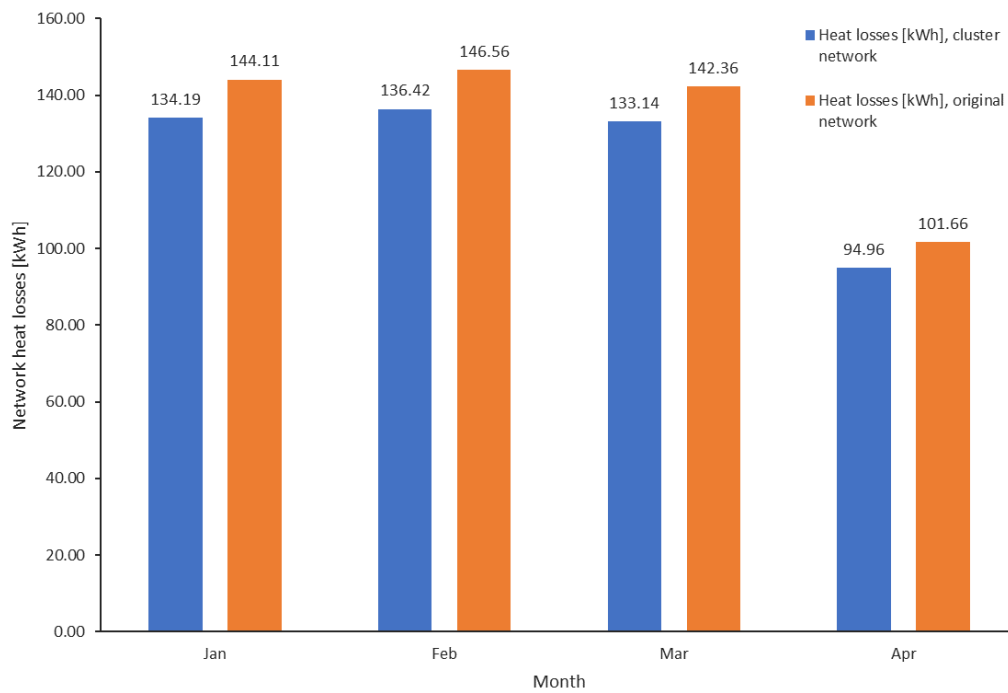
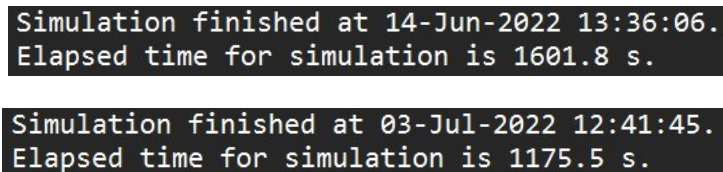


Figure 6.9: Comparison between monthly heat losses between original and equivalent networks.

In this plot are presented the monthly heat losses among the clustered network (in blue) and the original one (in orange). The heat losses of April are considered only for the first two weeks of the month, because the simulation ended in the 15th April, due to the heating period assumed.

The columns indicates the difference of monthly heat losses because of the reason mentioned above, which explained the conservation of the main features between the two networks only for design conditions, during out-of-design conditions the results can vaguely change. In this case the difference is about 9.3% in all the month examined, that is considered a reasonable standard in this field.

At least, the comparison between the computational time taken by NeMo for the simulation of the clustered network and the initial one is presented in the next picture:



```
Simulation finished at 14-Jun-2022 13:36:06.
Elapsed time for simulation is 1601.8 s.

Simulation finished at 03-Jul-2022 12:41:45.
Elapsed time for simulation is 1175.5 s.
```

Figure 6.10: Computational time taken by NeMo for a) Original network, b) Equivalent network

To analyse the networks, NeMo has taken 1601.8 [s] for the initial one, and 1175.5 [s] for the other one, despite a slight reduction of 15% of the nodes and branches, and about 7% of the total length, i.e. from 7.8 km to 7.3 km. Converting the computational time in minutes:

$$\frac{1601.8}{60} = 26.69 \text{ min}$$

$$\frac{1175.5}{60} = 19.59 \text{ min}$$

It can be noticed the huge reduction of approximately 7 minute for the elapsed time, that represents more than 25%.

Chapter 7

Conclusions

This work has been divided in several parts: the first part consists of the introduction with an overview on the DHC system, the physical models used to predict the behaviour of the networks, and the utility of the clustering in DHC networks. The second part and the third part focus on the functioning of *NeMo* and Eurac model, evaluating these tools accuracy, and introducing important parameters such as time and space discretization, Courant number for *NeMo*, and the maximum number of particles inside the ducts for a certain time-step of the Detailed Model. These parameters allow the user to create different accuracy outlet profiles in order to fit a theoretical solution.

The fourth one is the main part, concentrating on the real Aalborg network, and the filling of *NeMo* input, with the aim of starting the simulation of the network. The DHN consists of 158 nodes and 157 branches, it is located in the Aalborg campus as part of a larger net distributed all over the city of Aalborg, where the main supplier is a cement factory. In the near future, the campus network is expected to integrate waste heat from a Data Centre, though this possibility was not explicitly discussed in this work. The peak power of the considered network is 34.94 MW, the total heat losses per month are 144.11 MWh for January, 146.56 MWh for February, 142.36 MWh for March, and 101.66 MWh for April, while the total length is about 7.8 km, the total water volume is 167.82 m³.

The results obtained from the simulation tool *NeMo* are in line with the expectations. The analysis was focused on heat losses between the supply station and one of the critical nodes (chosen for the ID node 48), as well as on, other features such as the thermal inertia of the fluid and thermal power.

The fifth part is related to the clustering function implemented in MATLAB and applied to the original Aalborg network, that allows diminishing the number of nodes and branches. A test with a reduction of about 15%, in the number of nodes and about 7%, in the total length was carried out. This cut brings a significant decrease of the elapsed time for the simulation, i.e., more than 25%, from 26.69 min to 20 min. After the new labelling of the equivalent network, the ID node 39 (ex 48) was compared to the old ID node 48, to check the conservation of the main features. This is exactly confirmed for the nominal conditions, as the method is

designed to respect this constraint. Out of the design conditions, the main features exhibit a limited change, as demonstrated in figure 6.7, where the outlet temperature reached by the water is about 76.16°C instead of 76.08°C, and in figure 6.10, where it is represented the difference of 9.3% between the network heat losses of the equivalent network, from the original one, that can still be considered acceptable under 15-20%.

The next steps that can be followed from this work are:

- Analysis, with the simulation tools exploited in this thesis, of the impact of additional waste heat sources such as a Data Centre of Aalborg University, in order to evaluating the temperature parameters of the net, and how they can affect, for example, the efficiency of the network.
- Automatization of the application of the MATLAB functions of step 1 and 2, exploring the network graph with suitable search algorithms.
- Analysis of more extended clustering cases, e.g., reducing the number of nodes and branches by 50% or more, to study in more detail the interplay between reduction of computational time and of accuracy, identify suitable compromises.

References

- ¹ Mehmet Ali Alkan, Ali Keçebaş, e Nurettin Yamankaradeniz, «Exergoeconomic Analysis of a District Heating System for Geothermal Energy Using Specific Exergy Cost Method», *Energy* 60 (October 2013): 426–34, <https://doi.org/10.1016/j.energy.2013.08.017>.
- ² Alemayehu Gebremedhin, «Optimal Utilisation of Heat Demand in District Heating System—A Case Study», *Renewable and Sustainable Energy Reviews* 30 (February 2014): 230–36, <https://doi.org/10.1016/j.rser.2013.10.009>.
- ³ Directive (EU) 2018/844 of the European Parliament and of the council of 30 May 2018 amending Directive 2010/31/EU on the energy performance of buildings and Directive 2012/27/EU on energy efficiency.
- ⁴ Lund H, Werner S, Wiltshire R, Svendsen S, Thorsen JE, Hvelplund F, et al. 4th Generation District Heating (4GDH): Integrating smart thermal grids into future sustainable energy systems. *Energy* 2014;68:1–11. <https://doi.org/10.1016/J.ENERGY.2014.02.089>
- ⁵ European Commission. Joint Research Centre, and European Technology Platform on Renewable Heating and Cooling (RHC-Platform), 2020–2030–2050, common vision for the renewable heating and cooling sector in Europe: European technology platform on renewable heating and cooling. Luxembourg: EUR-OP; 2011.
- ⁶ Pezzutto S, Fazeli R, De Felice M, Sparber W. Future development of the air-conditioning market in Europe: an outlook until 2020. *Wiley Interdiscip Rev Energy Environ* 2016;5(6):649–69.
- ⁷ Dario Prando et al., «Analysis of the Energy and Economic Impact of Cost-Optimal Buildings Refurbishment on District Heating Systems», *Science and Technology for the Built Environment* 21, n. 6 (18 august 2015): 876–91, <https://doi.org/10.1080/23744731.2015.1040343>.
- ⁸ Werner S, Frederiksen S. District heating and cooling. 1st ed. Studentlitteratur AB; 2013.
- ⁹ Stefan Forsaeus Nilsson et al., «Sparse District-Heating in Sweden», *Applied Energy* 85, n. 7 (luglio 2008): 555–64, <https://doi.org/10.1016/j.apenergy.2007.07.011>.

¹⁰ Charlotte Reidhavs e Sven Werner, «Profitability of Sparse District Heating», *Applied Energy* 85, n. 9 (September 2008): 867–77, <https://doi.org/10.1016/j.apenergy.2008.01.006>.

¹¹ Henrik Lund et al., «4th Generation District Heating (4GDH)», *Energy* 68 (April 2014): 1–11, <https://doi.org/10.1016/j.energy.2014.02.089>.

¹² Simone Buffa et al., «5th Generation District Heating and Cooling Systems: A Review of Existing Cases in Europe», *Renewable and Sustainable Energy Reviews* 104 (April 2019): 504–22, <https://doi.org/10.1016/j.rser.2018.12.059>.

¹³ <https://www.life4heatrecovery.eu/>

¹⁴ Palsson H, Bohm B. Methods for planning and operating decentralized combined heat and power plants. PhD Thesis. Riso & DTU - Department of Energy Engineering (ET); 2000.

¹⁵ Benonysson A, Bohm B, Ravn HF. Operational optimization in a district heating system. *Energy Convers Manag* 1995;36:297–314. [https://doi.org/10.1016/0196-8904\(95\)98895-T](https://doi.org/10.1016/0196-8904(95)98895-T).

¹⁶ Grosswindhager S, Voigt A, Kozek M. Linear finite-difference schemes for energy transport in district heating networks; 2011.

¹⁷ Gabrielaitiene I, Sunden B, Kacianauskas R, Bohm B. Dynamic modelling of the thermal performance of district heating pipelines 2003:185–92.

¹⁸ A. Dénarié, M. Aprile, e M. Motta, «Heat Transmission over Long Pipes: New Model for Fast and Accurate District Heating Simulations», *Energy* 166 (January 2019): 267–76, <https://doi.org/10.1016/j.energy.2018.09.186>.

¹⁹ Jean Duquette, Andrew Rowe, e Peter Wild, «Thermal Performance of a Steady State Physical Pipe Model for Simulating District Heating Grids with Variable Flow», *Applied Energy* 178 (settembre 2016): 383–93, <https://doi.org/10.1016/j.apenergy.2016.06.092>.

²⁰ Vladimir D. Stevanovic et al., «Prediction of Thermal Transients in District Heating Systems», *Energy Conversion and Management* 50, n. 9 (September 2009): 2167–73, <https://doi.org/10.1016/j.enconman.2009.04.034>.

²¹ Yaran Wang et al., «Thermal Transient Prediction of District Heating Pipeline: Optimal Selection of the Time and Spatial Steps for Fast and Accurate

Calculation», *Applied Energy* 206 (novembre 2017): 900–910, <https://doi.org/10.1016/j.apenergy.2017.08.061>.

²² Basak Falay et al., «Enabling Large-Scale Dynamic Simulations and Reducing Model Complexity of District Heating and Cooling Systems by Aggregation», *Energy* 209 (October 2020): 118410, <https://doi.org/10.1016/j.energy.2020.118410>.

²³ Helge V. Larsen et al., «Aggregated Dynamic Simulation Model of District Heating Networks», *Energy Conversion and Management* 43, n. 8 (May 2002): 995–1019, [https://doi.org/10.1016/S0196-8904\(01\)00093-0](https://doi.org/10.1016/S0196-8904(01)00093-0).

²⁴ Selva Calixto, Marco Cozzini, e Giampaolo Manzolini, «Modelling of an Existing Neutral Temperature District Heating Network: Detailed and Approximate Approaches», *Energies* 14, n. 2 (12 gennaio 2021): 379, <https://doi.org/10.3390/en14020379>.

²⁵ J. Vivian et al., «The Effect of Discretization on the Accuracy of Two District Heating Network Models Based on Finite-Difference Methods», *Energy Procedia* 149 (Settembre 2018): 625–34, <https://doi.org/10.1016/j.egypro.2018.08.227>.

²⁶ Enrico Pratavia et al., «EURCA: An Open-Source Urban Building Energy Modelling Tool for the Efficient Evaluation of Cities Energy Demand», *Renewable Energy* 173 (Agosto 2021): 544–60, <https://doi.org/10.1016/j.renene.2021.03.144>.

Appendix

MATLAB code

SCRIPT 1:

```
%clusterstep1
Tsupply=85; %Related to the P_peak (which is verify in winter conditions,
minimum T_outdoor) [°C]
Treturn=45; %constant value for the Aalborg Network (assumption) [°C]
cp_w=4.187; %specific heat of water [kJ/kg K]
rho_w=997; %water density [kg/m^3]
cp_p=0.502; %specific heat of steel [kJ/kg K]
rho_p=7930; %density of steel 304 [kg/m^3]
T_G=2.55406; %minimum temperature of the ground required for the P_peak
[°C]
T_s=Tsupply;
phi_1=1;
phi_2=2;

%node_matrix= readmatrix ("Node Matrix per automatizzazione
processo.xlsx", "Range", "C3:D160");
node_matrix= readmatrix ("Nuova Matrice Nodi.xlsx", "Range", "A1:B158");

for i_v=1:158
    v(i_v).P=node_matrix(i_v,1);
    v(i_v).m=node_matrix(i_v,2);
end

%pipe_matrix= readmatrix ("Pipe Matrix per automatizzazione
processo.xlsx", "Range", "C4:Q160");
pipe_matrix= readmatrix ("Nuova Matrice Tubi.xlsx", "Range", "A1:O157");
%incidence_matrix= readmatrix("Incidence Matrix per automatizzazione
processo.xlsx", "Range", "B3:C159");
incidence_matrix= readmatrix("Nuova Matrice Incidenza.xlsx", "Range",
"A1:B157");

for i_e=1:157
    e(i_e).d=pipe_matrix(i_e,2);
    e(i_e).D=pipe_matrix(i_e,6);
    e(i_e).A=pipe_matrix(i_e,12);
    e(i_e).L=pipe_matrix(i_e,1);
    e(i_e).V=pipe_matrix(i_e,9);
    e(i_e).tau=pipe_matrix(i_e,14);
    e(i_e).v=pipe_matrix(i_e,15);
    e(i_e).Hs=pipe_matrix(i_e,10);
    e(i_e).Hr=pipe_matrix(i_e,11);
    e(i_e).Tr=pipe_matrix(i_e,13);
```

```

    e(i_e).v_ini=incidence_matrix(i_e,1);
    e(i_e).v_fin=incidence_matrix(i_e,2);
end

i_v1=...; %ID NODE 1
i_v2=...; %ID NODE 2
i_e1=...; %ID EDGE 1
i_e2=...; %ID EDGE 2
v_in=v([i_v1 i_v2]);
e_in=e([i_e1 i_e2]);

if e(i_e1).tau<=e(i_e2).tau

[v_out,e_out,P_G,T_AB,teta_Ar,teta_Br]=clusterstep1finale(v_in,e_in,Tsupply,
Treturn,cp_w,rho_w,cp_p,rho_p,T_G,T_s,phi_1,phi_2)
else
    fprintf ("Switch the definition 1 and 2 of nodes and pipes because
tau1>tau2! \n ")
end

perdite_A_B=(T_s-T_G)*(e_out(1).Hs+e_out(2).Hs)+(T_AB-
T_G)*e_out(1).Hr+(e_out(2).Tr-T_G)*e_out(2).Hr
perdite_1_2=(T_s-T_G)*(e_in(1).Hs+e_in(2).Hs)+(e_in(1).Tr-
T_G)*e_in(1).Hr+(e_in(2).Tr-T_G)*e_in(2).Hr
volumi_A_B=e_out(1).V+e_out(2).V
volumi_1_2=e_in(1).V+e_in(2).V

e(i_e1)=e_out(1);
e(i_e2)=e_out(2);
v(i_v1)=v_out(1);
v(i_v2)=v_out(2);

for i_e=[i_e1,i_e2]
    pipe_matrix(i_e,2)=e(i_e).d;
    pipe_matrix(i_e,6)=e(i_e).D;
    pipe_matrix(i_e,12)=e(i_e).A;
    pipe_matrix(i_e,1)=e(i_e).L;
    pipe_matrix(i_e,9)=e(i_e).V;
    pipe_matrix(i_e,14)=e(i_e).tau;
    pipe_matrix(i_e,15)=e(i_e).v;
    pipe_matrix(i_e,10)=e(i_e).Hs;
    pipe_matrix(i_e,11)=e(i_e).Hr;
    pipe_matrix(i_e,13)=e(i_e).Tr;
    incidence_matrix(i_e,1)=e(i_e).v_ini;
    incidence_matrix(i_e,2)=e(i_e).v_fin;
end

for i_v=[i_v1,i_v2]
    node_matrix(i_v,1)=v(i_v).P;
    node_matrix(i_v,2)=v(i_v).m;
end
writematrix(pipe_matrix, "Nuova Matrice Tubi.xlsx");
writematrix(node_matrix, "Nuova Matrice Nodi.xlsx");
writematrix(incidence_matrix, "Nuova Matrice Incidenza.xlsx");

```

SCRIPT 2:

```
%function clusterstep1finale
```

```
function
```

```
[v_out,e_out,P_G,T_AB,teta_Ar,teta_Br]=clusterstep1finale(v_in,e_in,Tsupply,Treturn,cp_w,rho_w,cp_p,rho_p,T_G,T_s,phi_1,phi_2)
```

```
v_out=v_in;  
e_out=e_in;
```

```
%calculation
```

```
e_out(1).tau=e_in(1).tau %time delay in branch A is equal to the  
delay in branch 1
```

```
e_out(2).tau=e_in(2).tau-e_in(1).tau %time delay in branches A e B is  
equal to the delay in branch 2
```

```
alfa=v_in(2).m/v_in(1).m
```

```
%phi=C_w/(C_w+C_p); %ignoring the steel pipe is equivalent to assign  
the value 1 to the variables "phi" and "psi"
```

```
phi_A=1; %phi_A=phi_1
```

```
phi_B=1; %phi_B=phi_2
```

```
%psi=phi_2/phi_1;
```

```
psi=1;
```

```
%V_A+e_out(2).V=e(1).V+e(2).V the water volume is conserved
```

```
%m_A+m_B=v(1).m+v(2).m the mass flow is conserved
```

```
%v_out(1).P+v_out(2).P=v(1).P+v(2).P the heat load is conserved
```

```
%Q_A+Q_B=Q_1+Q_2 the heat loss is conserved
```

```
%To obtain the equivalent network, we choose Branch B equal to the  
last part of branch 2
```

```
%This choice does not take the insulation of pipe B into account
```

```
e_out(2).d=e_in(2).d; %inner diameter of the steel pipe
```

```
e_out(2).D=e_in(2).D; %outer diameter of the steel pipe
```

```
e_out(2).A=e_in(2).A; %cross section of the pipe
```

```
phi_B=phi_2;
```

```
v_out(2).m=v_in(2).m; %mass flow in branch B is equal to that in  
branch 2
```

```
e_out(1).v=(v_in(1).m*e_in(1).v+v_in(2).m*e_in(2).v)/(v_in(1).m+v_in(2).m)
```

```
%velocity in branch A equals to a weighted average of the velocities in  
branches 1 and 2
```

```
v_out(1).m=v_in(1).m;
```

```
e_out(1).V=e_in(1).V*(1+alfa)*(phi_A/phi_1) %volume in the branch A
```

```
gamma=(e_in(1).V/e_in(2).V)*alfa;
```

```
e_out(2).V=e_in(2).V*(1-gamma*psi) %volume in the branch B
```

```
e_out(2).L=e_in(2).L*(1-gamma*psi) %length of the branch B
```

```
e_out(2).v=e_out(2).L/e_out(2).tau
```

```
beta=1+alfa;
```

```

    e_out(1).L=e_in(1).L*(1+(alfa^2)*psi*(e_in(1).A/e_in(2).A))/beta
%length of the branch A

e_out(1).d=2*sqrt((beta*(1+alfa*psi)*e_in(1).A*e_in(2).A)/((e_in(2).A+e_in
(1).A*(alfa^2)*psi)*pi)) %inner diameter of the steel pipe in branch A
    e_out(1).D=e_out(1).d*sqrt(1+((rho_w*cp_w)/(rho_p*cp_p))*((1-
phi_A)/phi_B)) %outer diameter of the steel pipe in branch A
    e_out(1).A=pi*((e_out(1).d/2)^2)

    e_out(1).v_ini=e_in(1).v_ini;
    e_out(1).v_fin=e_in(1).v_fin;
    e_out(2).v_ini=e_in(1).v_fin;
    e_out(2).v_fin=e_in(2).v_fin;

    %inner and outer diameter of branch B is already known.

    %INCLUDING THERMAL HEAT LOSSES

    %To this point, the insulation of the pipes has been excluded from the
calculations

    %When calculating the heat loss from a pipe, we use the temperature at
the inlet to the pipe
    %Since the heat loss in a pipe and the temperature drop along the pipe
are small
    %the error introduced by using the inlet temperature is acceptable

    %Define:
    %e(1).Tr,e(2).Tr,T_G (=T_groung),T_s
(=T_supply),e(2).Hr,e(1).Hr,e(1).Hs,e(2).Hs

    %e_out(1).Tr is the return temperature from the load in node A before
mixing with the water branch B
    %T_AB is the temperature in node A after mixing has taken place

    %calculation
    P_G=v_in(2).m*(T_s-T_G)*cp_w
    T_AB=(e_in(1).Tr+alfa*e_in(2).Tr)/beta %both networks have the same
return temperature in node 0

    %heat conductivity from branch B

    e_out(2).Hr=e_in(2).Hr*(1-gamma*psi)

    %Conservation of heat loss can be expressed as:
    %(T_AB-T_G)*e_out(1).Hr+(e_out(2).Tr-T_G)*e_out(2).Hr=(e(1).Tr-
T_G)*e(1).Hr+(e(2).Tr-T_G)*e(2).Hr

    DeltaT1=e_in(1).Tr-T_G;
    DeltaT2=e_in(2).Tr-T_G;
    DeltaT_B=DeltaT2;
    DeltaT_AB=(DeltaT1+alfa*DeltaT2)/beta;

```

```

e_out(1).Hr=((DeltaT1*e_in(1).Hr+DeltaT2*e_in(2).Hr*gamma*psi)*beta)/(DeltaT1+alfa*DeltaT2)
    e_out(2).Hs=e_in(2).Hs*(1-gamma*psi)
    e_out(1).Hs=e_in(1).Hs+(gamma*psi*e_in(2).Hs)

    teta_Ar=e_out(1).Hr/e_in(1).Hr
    teta_Br=e_out(2).Hr/e_in(1).Hr
    teta_2r=e_in(2).Hr/e_in(1).Hr

    %We define from the previous equation:

    e_out(1).Tr=e_in(1).Tr*(((teta_Ar*alfa/beta)+teta_Br-
    alfa)/teta_Br)+e_in(2).Tr*(((teta_Ar*alfa/beta)+teta_Br-
    teta_2r)*alfa)/(teta_Br)+T_G*((1+teta_2r-teta_Ar-teta_Br)*alfa/teta_Br)
    e_out(2).Tr=e_in(1).Tr*((1-
    (teta_Ar/beta))/(teta_Br))+e_in(2).Tr*((teta_2r-
    (teta_Ar*alfa/beta))/(teta_Br))+T_G*((teta_Ar+teta_Br-teta_2r-1)/teta_Br)

    %The heat loads v_out(1).P and v_out(2).P in the equivalent network,
    can be stated as linear expression in v(1).P and v(2).P

    %v(1).P=v(1).m*(T_s-e(1).Tr)*cp_w  dovrei conoscerla
    e_in(1).Tr=T_s-(v_in(1).P/(v_in(1).m*cp_w));

    %v(2).P=v(2).m*(T_s-e(2).Tr)*cp_w  dovrei conoscerla
    e_in(2).Tr=T_s-(v_in(2).P/(v_in(2).m*cp_w));

    %v_out(2).P=m_B*(T_s-e_out(2).Tr)*c_w
    v_out(2).P=v_in(1).P*((alfa*(1-
    (teta_Ar/beta)))/teta_Br)+v_in(2).P*((teta_2r-
    (teta_Ar*alfa/beta))/teta_Br)+P_G*((teta_Ar+teta_Br-teta_2r-1)/teta_Br)

    %where P_G=v(2).m*(T_s-T_G)*c_w
    %by using the fact that the total heat load in the equivalent network
    should equal the total load in the original network
    (v_out(1).P+v_out(2).P=v(1).P+v(2).P)

    v_out(1).P=v_in(1).P*(((teta_Ar*alfa/beta)+teta_Br-
    alfa)/teta_Br)+v_in(2).P*((teta_Ar*alfa/beta)+teta_Br-teta_2r)/(teta_Br)-
    P_G*((teta_Ar+teta_Br-teta_2r-1)/teta_Br)

```

SCRIPT 3:

```
%removeinternalnodesinput
```

```
%input
```

```
rho_p=7930; %density of acciaio inox 304 [kg/m^3]
```

```
cp_p=0.502; %specific heat of steel [kJ/kg K]
```

```
rho_w=997; %water density [kg/m^3]
```

```
cp_w=4.187; %specific heat of water [kJ/kg K]
```

```
X=(rho_p*cp_p)/(rho_w*cp_w);
```

```
phi_1=1;
```

```
phi_2=1;
```

```
phi_3=1;
```

```
M_NMT=readmatrix ("Nuova Matrice Tubi.xlsx","Range","A1:O157");
```

```
M_NMN=readmatrix ("Nuova Matrice Nodi.xlsx","Range","A1:B158");
```

```
i_e1=...;
```

```
i_e2=...;
```

```
i_e3=...;
```

```
i_v1=...;
```

```
i_v2=...;
```

```
i_v3=...;
```

```
i_v4=...;
```

```
e(1).d=M_NMT(i_e1,2); % [m] inner diameter of steel pipe 1
```

```
e(1).D=M_NMT(i_e1,6); % [m] outer diameter of steel pipe 1
```

```
e(1).mu=M_NMN(i_v2,2)+M_NMN(i_v3,2)+M_NMN(i_v4,2); %mass flow rate of the  
pipe 1
```

```
e(1).L=M_NMT(i_e1,1); % [m] %pipe 1 length
```

```
e(1).V=(1/4)*pi*e(1).L*(e(1).d)^2; % [m^3] water volume of the pipe 1
```

```
e(1).tau=(rho_w*e(1).V)/(e(1).mu*phi_1); %time delay in branch 1 [s]
```

```
e(1).V_p=(1/4)*pi*e(1).L*(e(1).D)^2-e(1).V;
```

```
e(1).h_s=M_NMT(i_e1,10)/e(1).L;
```

```
e(2).d=M_NMT(i_e2,2); % [m] inner diameter of steel pipe 2
```

```
e(2).D=M_NMT(i_e2,6); % [m] outer diameter of steel pipe 2
```

```
e(2).mu=M_NMN(i_v3,2)+M_NMN(i_v4,2); %mass flow rate of the pipe 2
```

```
e(2).L=M_NMT(i_e2,1); % [m] %pipe 2 length
```

```
e(2).V=(1/4)*pi*e(2).L*(e(2).d)^2; % [m^3] water volume of the pipe 2
```

```
e(2).tau=(rho_w*e(2).V)/(e(2).mu*phi_2); %time delay in branch 2 [s]
```

```
e(2).V_p=(1/4)*pi*e(2).L*(e(2).D)^2-e(2).V;
```

```
e(2).h_s=M_NMT(i_e2,10)/e(2).L;
```

```
e(3).d=M_NMT(i_e3,2); % [m] inner diameter of steel pipe 3
```

```
e(3).D=M_NMT(i_e3,6); % [m] outer diameter of steel pipe 3
```

```
e(3).mu=M_NMN(i_v4,2); % [kg/s] mass flow rate of the pipe 3
```

```
e(3).L=M_NMT(i_e3,1); % [m] %pipe 3 length
```

```
e(3).V=(1/4)*pi*e(3).L*(e(3).d)^2; % [m^3] water volume of the  
pipe 3
```

```
e(3).tau=(rho_w*e(3).V)/(e(3).mu*phi_3); %time delay in branch 3 [s]
```

```
e(3).V_p=(1/4)*pi*e(3).L*(e(3).D)^2-e(3).V;
```

```

e(3).h_s=M_NMT(i_e3,10)/e(3).L;

v(1).m=e(1).mu-e(2).mu; %mass flow rate of node 1
v(2).m=e(2).mu-e(3).mu; %mass flow rate of node 2

%M_P_in=readmatrix
("Loads_2520_ore_removalnodes.xlsx","Sheet","heatload_2520", "Range",
"B2:FC2521");
M_P_in=readmatrix ("Nuova Matrice Potenze.xlsx", "Range", "A1:FB2520");

%M_m_in=readmatrix("Loads_2520_ore_removalnodes.xlsx", "Sheet",
"massflowrate_2520", "Range", "B2:FC2521");
M_m_in=readmatrix("Nuova Matrice Portate.xlsx","Range", "A1:FB2520");

F_masspeak_in=readmatrix ("Nuova Matrice Nodi.xlsx", "Range", "B1:B158");
F_powerpeak_in=readmatrix ("Nuova Matrice Nodi.xlsx", "Range", "A1:A158");

% Call the function (defined in another file)

[v_out,e_out,fA,fB,gAA,gAB,gBB,gBA,M_P_out,M_m_out,F_masspeak_out,F_powerp
eak_out]=removeinternalnodesbackup(v,e,rho_p,cp_p,rho_w,cp_w,phi_1,phi_2,p
hi_3,M_P_in,M_m_in,F_masspeak_in,F_powerpeak_in)

writematrix (M_P_out, "Nuova Matrice Potenze.xlsx");
writematrix (M_m_out, "Nuova Matrice Portate.xlsx");
writematrix (F_powerpeak_out,"Nuova Matrice Nodi.xlsx","Range","A1:A158");
writematrix (F_masspeak_out,"Nuova Matrice Nodi.xlsx","Range","B1:B158");

M_NMT(i_e1,2)=e_out(1).d;    %[m] inner diameter of steel pipe 1 out
M_NMT(i_e1,6)=e_out(1).D;    %[m] outer diameter of steel pipe 1 out
M_NMT(i_e1,1)=e_out(1).L;    %[m] %pipe 1 out length
M_NMT(i_e1,9)=e_out(1).V;    %[m^3] water volume of the pipe 1 out
M_NMT(i_e1,14)=e_out(1).tau; %time delay in branch 1 out [s]
%e(1).V_p=(1/4)*pi*e(1).L*(e(1).D)^2-e(1).V;
M_NMT(i_e1,10)=e_out(1).h_s*e_out(1).L;
M_NMT(i_e1,11)=M_NMT(i_e1,10);
M_NMT(i_e1,15)=e_out(1).L/e_out(1).tau;
M_NMT(i_e1,12)=e_out(1).V/e_out(1).L;

M_NMT(i_e3,2)=e_out(2).d;    %[m] inner diameter of steel pipe 2 out
M_NMT(i_e3,6)=e_out(2).D;    %[m] outer diameter of steel pipe 2 out
M_NMT(i_e3,1)=e_out(2).L;    %[m] %pipe 2 out length
M_NMT(i_e3,9)=e_out(2).V;    %[m^3] water volume of the pipe 2 out
M_NMT(i_e3,14)=e_out(2).tau; %time delay in branch 2 out [s]
%e(1).V_p=(1/4)*pi*e(2).L*(e(1).D)^2-e(1).V;
M_NMT(i_e3,10)=e_out(2).h_s*e_out(2).L;
M_NMT(i_e3,11)=M_NMT(i_e3,10);
M_NMT(i_e3,15)=e_out(2).L/e_out(2).tau;
M_NMT(i_e3,12)=e_out(2).V/e_out(2).L;

M_NMT(i_e2,:)=-1000;
writematrix (M_NMT, "Nuova Matrice Tubi.xlsx");

```

SCRIPT 4:

```
%function removinginternalnodes
```

```
function
```

```
[v_out,e_out,fA,fB,gAA,gAB,gBB,gBA,M_P_out,M_m_out,F_masspeak_out,F_powerpeak_out]=removeinternalnodesbackup(v_in,e_in,rho_p,cp_p,rho_w,cp_w,phi_1,phi_2,phi_3,M_P_in,M_m_in,F_masspeak_in,F_powerpeak_in)
```

```
%mu indicates flow in the branches, while m, indicates flow to heat exchangers
```

```
phi_A=1;
```

```
phi_B=1;
```

```
X=(rho_p*cp_p)/(rho_w*cp_w);
```

```
v_out(1).m=e_in(1).mu-e_in(2).mu;
```

```
v_out(2).m=e_in(2).mu-e_in(3).mu;
```

```
fA=v_in(2).m/(v_in(1).m+v_in(2).m);
```

```
fB=1-fA;
```

```
gAA=(fA*e_in(2).tau)/(e_in(1).tau+fA*e_in(2).tau);
```

```
gAB=e_in(1).tau/(e_in(1).tau+fA*e_in(2).tau);
```

```
gBB=(fB*e_in(2).tau)/(e_in(3).tau+fB*e_in(2).tau);
```

```
gBA=e_in(3).tau/(e_in(3).tau+fB*e_in(2).tau);
```

```
e_out(1).mu=e_in(1).mu-gAA*v_in(1).m;
```

```
e_out(2).mu=e_in(2).mu-gBA*v_in(2).m;
```

```
e_out(1).L=e_in(1).L+fA*e_in(2).L
```

```
e_out(2).L=e_in(3).L+fB*e_in(2).L
```

```
e_out(1).tau=e_in(1).tau+fA*e_in(2).tau
```

```
e_out(2).tau=e_in(3).tau+fB*e_in(2).tau
```

```
e_out(1).V=e_in(1).V*(e_out(1).mu/e_in(1).mu)*(phi_A/phi_1)+fA*e_in(2).V*(e_out(1).mu/e_in(2).mu)*(phi_A/phi_2)
```

```
e_out(2).V=e_in(3).V*(e_out(2).mu/e_in(3).mu)*(phi_B/phi_3)+fB*e_in(2).V*(e_out(2).mu/e_in(2).mu)*(phi_B/phi_2)
```

```
%Except for phi_A, all variables on the right side are known
```

```
%phi_A=1/(1+X*((e_in(1).V_p+fA*e_in(2).V_p)/(e_in(1).V+fA*e_in(2).V)))
```

```
e_out(1).V_p=e_out(1).V*((1-phi_A)/(phi_A*X))
```

```
e_out(2).V_p=e_out(2).V*((1-phi_B)/(phi_B*X))
```

```
e_out(1).d=2*sqrt(e_out(1).V/(pi*e_out(1).L))
```

```
e_out(2).d=2*sqrt(e_out(2).V/(pi*e_out(2).L))
```

```
e_out(1).D=2*sqrt((e_out(1).V+e_out(1).V_p)/(pi*e_out(1).L))
```

```
e_out(2).D=2*sqrt((e_out(2).V+e_out(2).V_p)/(pi*e_out(2).L))
```

%assuming constant temperature, preservation of heat loss is expressed by:

```
e_out(1).h_s=(e_in(1).h_s*e_in(1).L+fA*e_in(2).h_s*e_in(2).L)/e_out(1).L
e_out(2).h_s=(e_in(3).h_s*e_in(3).L+fB*e_in(2).h_s*e_in(2).L)/e_out(2).L

verificavolumi_1_2_3=e_in(1).V+e_in(2).V+e_in(3).V
verificavolumi_A_B=e_out(1).V+e_out(2).V

verificaportate_m1_m2=v_out(1).m+v_out(2).m
verificaportatesplittate=v_out(1).m*gAA+v_out(1).m*gAB+v_out(2).m*gBA+v_out(2).m*gBB

i_v1=...;
i_v2=...;
i_v3=...;
i_v4=...;

M_P_out=M_P_in;
M_P_out(:,i_v2)=(M_P_in(:,i_v2)*gAB)+(M_P_in(:,i_v3)*gBA);%nodo centrale
ottenuto dalla fusione dei due centrali su quattro nodi
M_P_out(:,i_v3)=zeros(size(M_P_out,1),1); %il terzo nodo sparisce,
chiamiamo il nuovo nodo come il secondo, facciamo diventare la colonna del
terzo nodo originale una colonna di zeri
M_P_out(:,i_v1)=(M_P_in(:,i_v2)*gAA)+M_P_in(:,i_v1); %primo nodo della
nuova configurazione
M_P_out(:,i_v4)=(M_P_in(:,i_v3)*gBB)+M_P_in(:,i_v4); %ultimo nodo della
nuova configurazione

M_m_out=M_m_in;
M_m_out(:,i_v2)=(M_m_in(:,i_v2)*gAB)+(M_m_in(:,i_v3)*gBA);%nodo centrale
ottenuto dalla fusione dei due centrali su quattro nodi
M_m_out(:,i_v3)=zeros(size(M_m_out,1),1); %il terzo nodo sparisce,
chiamiamo il nuovo nodo come il secondo, facciamo diventare la colonna del
terzo nodo originale una colonna di zeri
M_m_out(:,i_v1)=(M_m_in(:,i_v2)*gAA)+M_m_in(:,i_v1); %primo nodo della
nuova configurazione
M_m_out(:,i_v4)=(M_m_in(:,i_v3)*gBB)+M_m_in(:,i_v4); %ultimo nodo della
nuova configurazione

F_masspeak_out=F_masspeak_in;
F_masspeak_out(i_v2)=(F_masspeak_in(i_v2)*gAB)+(F_masspeak_in(i_v3)*gBA);
F_masspeak_out(i_v3)=0;
F_masspeak_out(i_v1)=(F_masspeak_in(i_v2)*gAA)+F_masspeak_in(i_v1);
F_masspeak_out(i_v4)=(F_masspeak_in(i_v3)*gBB)+F_masspeak_in(i_v4);

F_powerpeak_out=F_powerpeak_in;
F_powerpeak_out(i_v2)=(F_powerpeak_in(i_v2)*gAB)+(F_powerpeak_in(i_v3)*gBA
);
F_powerpeak_out(i_v3)=0;
F_powerpeak_out(i_v1)=(F_powerpeak_in(i_v2)*gAA)+F_powerpeak_in(i_v1);
F_powerpeak_out(i_v4)=(F_powerpeak_in(i_v3)*gBB)+F_powerpeak_in(i_v4);
```

Ringraziamenti

Giunto alla fine di questo percorso che mi ha regalato tante emozioni, incontri, amicizie, soddisfazioni e momenti speciali, desidero ringraziare:

La mia famiglia, papà Ezio e mamma Daniela, perché mi hanno permesso di arrivare a questo enorme traguardo, essendo i miei primi sostenitori e spronandomi ogni giorno a dare il massimo, pur assecondando ogni mio momento di sconforto; mio fratello Marco, fonte di ispirazione e amico, sempre con la battuta pronta a rendere piacevole ogni momento passato insieme.

Marco C. ed il prof. Zarrella, per la loro gentilezza, disponibilità, competenza e intelligenza con cui mi hanno seguito e supportato in questi sei mesi di tirocinio, trovando sempre una soluzione tempestiva ai problemi, e per l'opportunità di lavorare presso un centro di ricerca di livello come Eurac Research, la cui esperienza mi ha permesso di crescere sotto tanti punti di vista. Tutto il gruppo SHC di Eurac, con il quale ho instaurato un rapporto di amicizia e stima fin da subito.

Jacopo, Enrico e Davide del gruppo di ricerca dell'università di Padova, che hanno sempre trovato il tempo per aiutarmi nonostante i loro impegni.

Irene, la mia ragazza e spalla destra da anni, che mi ha accompagnato in questo lungo percorso, svuotandomi la testa dai pensieri negativi, trasformandoli in felicità anche solo con un sorriso, un abbraccio, una passeggiata, una battuta o una canzone stonata cantata in macchina.

Giovanni L., amico di una vita, compagno di avventure e disavventure, sempre pronto a rincuorarmi e ad aiutarmi nel momento del bisogno, a regalarmi momenti di divertimento che non scorderò mai, pronto a passarne altrettanti di fantastici.

Tutta la compagnia di Fumane, a cui mi lega un rapporto che dura da quando abbiamo sei anni, con cui ho condiviso ogni tappa della mia vita finora, dai traguardi scolastici, alle serate indimenticabili, ai pomeriggi di calcio e fantacalcio, alle vacanze insieme. Non avrei potuto sceglierne di migliori.

Riccardo M., Giovanni A., Alessandro A., Emanuele M., Simone L., Alessandro L., Lorenzo Z., che nonostante siano entrati da poco nella mia vita, è come se li conoscessi da sempre tra risate, serate, domeniche di Serie A e Formula 1.

Giulio C., conosciuto in un pomeriggio di tutorato di Analisi 1 ad ottobre 2016, con cui ho condiviso il banco, gli esami, le lezioni e lo studio fino ad oggi, diventando molto più che un semplice compagno di corso, ma un grandissimo amico, con cui ho l'orgoglio di condividere questo giorno speciale per la seconda volta.

I miei coinquilini, Jacopo C., Christian G., Nicola P., Nicola B., con i quali ho passato ogni giorno della settimana per anni, tra studio, playstation, calcetti, pessime cene, insulti, risate, cene da Pippo, chilometri su chilometri a piedi e pandemie.

Alvise Z., Marta B., Emanuele D., Giacomo P., Silvia C., Chiara B., e tutti gli altri amici che sono sempre stati presenti in questi anni, mi hanno fatto sentire parte di loro fin da subito e con i quali resterò sempre affezionato.

Tutte le persone che Padova mi ha permesso di conoscere in questa esperienza, Fabio F., conosciuto in treno quasi per caso il primo anno e diventato nel tempo un grande amico, Angelica P., Giovanni C., Luca B., Andrea C., Jacopo P., e tutti gli altri, per aver contribuito anche ad un solo momento di felicità in questi anni.

Padova, città che mi ha cresciuto fino a questo giorno, assieme a tutto quello che ha da offrire ad uno studente, dalle mille aule studio, ai Navigli, alle ricolme piazze in ogni giorno dell'anno, ai concerti, ai calcetti, ai viaggi in tram e in treno, al Piovego ed al Portello.

Grazie.